Contributions to Mineralogy and Petrology (2024) 179:54
https://doi.org/10.1007/s00410-024-02138-9

ORIGINAL PAPER

A multi-methodological approach to record dynamics and timescales of the plumbing system of Zaro (Ischia Island, Italy)

Carlo Pelullo[1] · Sumit Chakraborty[2] · Chiara Paola Montagna[3] · Ilenia Arienzo[1] · Richard James Brown[4] · Massimo D'Antonio[5] · Sandro de Vita[1] · Claudia D'Oriano[3] · Manuela Nazzari[6] · Lucia Pappalardo[1] · Paola Petrosino[5]

Received: 30 October 2023 / Accepted: 19 April 2024 / Published online: 4 May 2024

Abstract

Determining the time spans of processes related to the assembly of eruptible magma at active volcanoes is fundamental to understand magma chamber dynamics and assess volcanic hazard. This information can be recorded in the chemical zoning of crystals. Nevertheless, this kind of study is still poorly employed for the active volcanoes of the Neapolitan area (Southern Italy), in particular, for Ischia island where the risk is extremely high and this information can provide the basis for probabilistic volcanic hazard assessment. For these reasons, we acquired chemical composition on clinopyroxene crystals erupted at Ischia during the Zaro eruption (6.6 ± 2.2 ka) and performed numerical simulations of the input of mafic magma into a trachytic reservoir, in order to investigate various aspects of pre-eruptive dynamics occurring at different timescales. This event emplaced a ~ 0.1 km^3 lava complex, in which the main trachytic lava flows host abundant mafic to felsic enclaves. Previous petrological investigation suggested that mafic magma(s) mixed/mingled with a trachytic one, before the eruption. In this work, the clinopyroxene zoning patterns depict the growth of crystals in different magmatic environments, recording sequential changes occurred in the plumbing system before the eruption. The evolution of the plumbing system involved a hierarchy of timescales: *a few hours* for magma mingling caused by mafic recharge(s) and likely occurred multiple times over *a decade* during which a dominant magmatic environment was sustained before the eruption. Such timescales must be considered in volcanic hazard assessment at Ischia and similar active volcanoes in densely populated areas.

Keywords Ischia island · Magma recharge · Numerical simulation · Clinopyroxene zoning pattern · Fe–Mg diffusion modelling

Communicated by Othmar Müntener.

✉ Carlo Pelullo
carlo.pelullo@ingv.it

[1] Istituto Nazionale di Geofisica e Vulcanologia, Sezione di Napoli Osservatorio Vesuviano, Via Diocleziano, 328, 80124 Naples, Italy

[2] Institut für Geologie, Mineralogie und Geophysik, Ruhr Universität Bochum, Universitätsstraße, 150, 44801 Bochum, Germany

[3] Istituto Nazionale di Geofisica e Vulcanologia, Sezione di Pisa, Via Cesare Battisti, 53, 56125 Pisa, Italy

[4] Department of Earth Sciences, Durham University, Science Labs, Durham DH1 3LE, UK

[5] Dipartimento di Scienze della Terra, dell'Ambiente e delle Risorse, Università di Napoli Federico II, Via Vicinale Cupa Cintia, 21, 80126 Naples, Italy

[6] Istituto Nazionale di Geofisica e Vulcanologia, Sezione di Roma 1, Via Di Vigna Murata, 605, 00143 Rome, Italy

Introduction

The investigation of magmatic processes occurring within sub-volcanic plumbing systems is crucial for volcanic hazard forecasting, given their role in triggering volcanic eruptions (Hildreth and Wilson 2007; Annen 2009; Kent et al. 2010; Druitt et al. 2012; Saunders et al. 2012; Allan et al. 2013; Sparks and Cashman 2017; Cooper 2019; Petrelli et al. 2023). Analysis of chemical zoning in minerals is one of the most efficient tools for investigating plumbing system dynamics (e.g., Zellmer et al. 1999, 2003; Humphreys et al. 2006; Ginibre et al. 2007; Costa and Chakraborty 2004; Streck 2008; Alves et al. 2009; Kahl et al. 2011, 2013; Ubide et al. 2015, 2019; Astbury et al. 2018; Solaro et al. 2020). Crystals respond texturally and compositionally to gradual or sudden changes in the magmatic system and preserve information regarding the crystallization conditions and the past history of magmatic processes and compositions (e.g.,

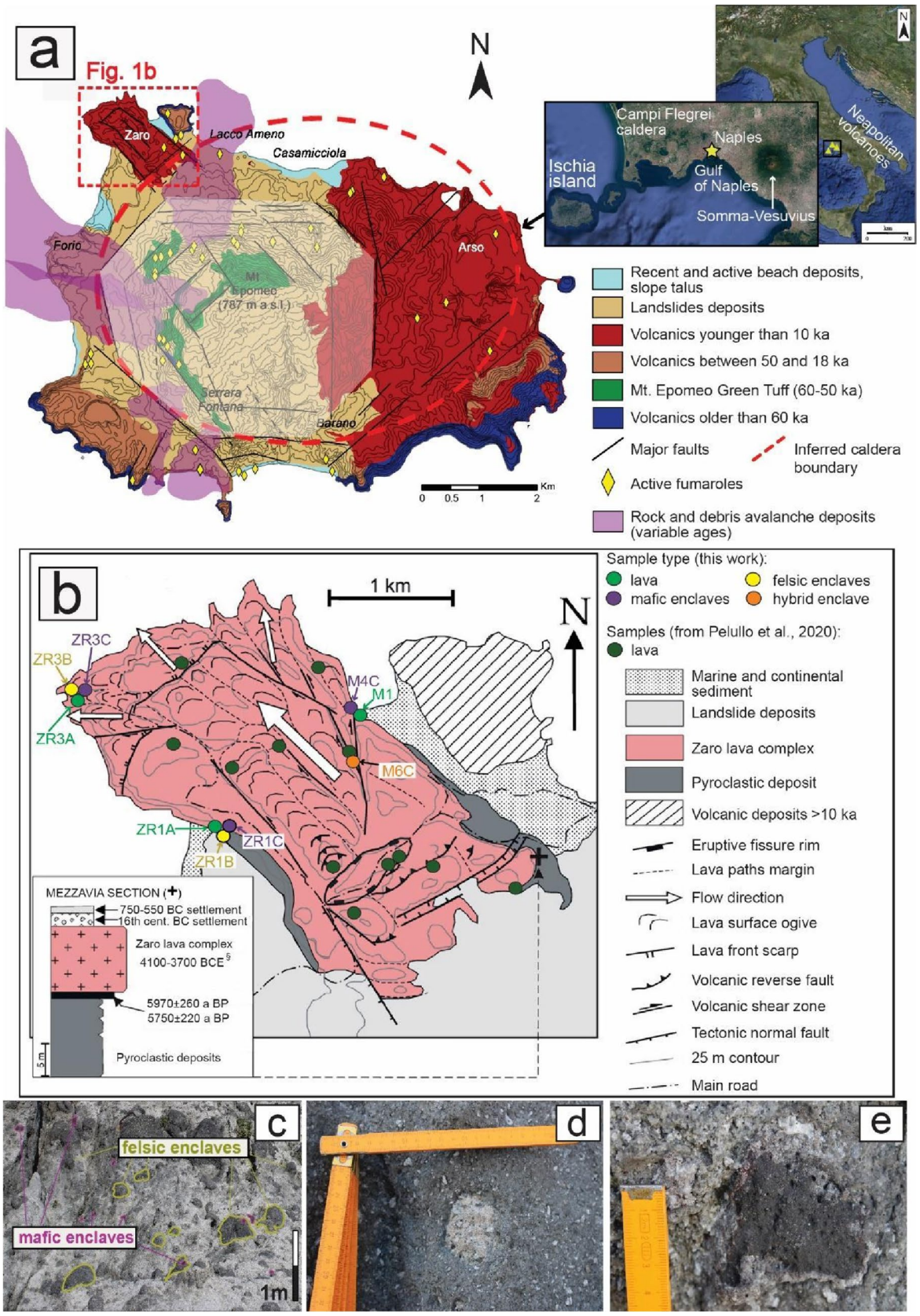
a
Fig. 1b
N
Zaro
Lacco Ameno
Casamicciola
Forio
Arso
Mt. Epomeo (787 m a.s.l.)
Serrara Fontana
Barano
0 0.5 1 2 Km
Campi Flegrei caldera
Naples
Ischia island
Gulf of Naples
Somma-Vesuvius
Neapolitan volcanoes
Recent and active beach deposits, slope talus
Landslides deposits
Volcanics younger than 10 ka
Volcanics between 50 and 18 ka
Mt. Epomeo Green Tuff (60-50 ka)
Volcanics older than 60 ka
Major faults
Inferred caldera boundary
Active fumaroles
Rock and debris avalanche deposits (variable ages)
b
1 km
N
ZR3C
ZR3B
ZR3A
M4C
M1
M6C
ZR1A
ZR1C
ZR1B
MEZZAVIA SECTION (+)
750-550 BC settlement
16th cent. BC settlement
Zaro lava complex
4100-3700 BCE§
5970±260 a BP
5750±220 a BP
Pyroclastic deposits
5 m
Sample type (this work):
lava
felsic enclaves
mafic enclaves
hybrid enclave
Samples (from Pelullo et al., 2020):
lava
Marine and continental sediment
Landslide deposits
Zaro lava complex
Pyroclastic deposit
Volcanic deposits >10 ka
Eruptive fissure rim
Lava paths margin
Flow direction
Lava surface ogive
Lava front scarp
Volcanic reverse fault
Volcanic shear zone
Tectonic normal fault
25 m contour
Main road
c
felsic enclaves
mafic enclaves
1m
d
e

◂**Fig. 1** **a** Geological sketch map of Ischia island (modified after Marotta et al. 2022); **b** geological map of the Zaro volcanic complex, showing the location of the sampled sites (modified after Vezzoli et al. 2009); **c** field evidence of felsic (yellow contours) and mafic (purple contours) enclaves hosted in the lava; **d** lava fragment hosted in felsic enclave in turn hosted in the lava; **e** mafic enclaves with cuspate borders

Putirka et al. 2003; Wallace and Bergantz 2002, 2004; Morgan and Blake 2006; Davidson et al. 2007; Ginibre et al. 2007; Kahl et al. 2015; Mangler et al. 2020). In particular, clinopyroxene crystallizes over a wide range of physico-chemical conditions (e.g., Putirka 2008; Mollo et al. 2018). Its compositions and textures have been extensively used for recording dynamics and timescales of pre-eruptive processes, such as magma crystallization, ascent, transport, storage, recharge, mixing and mush remobilization (e.g., Dunworth et al. 2001; Gioncada et al. 2005; Dohmen et al. 2017; Petrone et al. 2018, 2022; Ubide and Kamber 2018; Ubide et al. 2019; Bonechi et al. 2020, 2021; Di Stefano et al. 2020; Mangler et al. 2020; Mollo et al. 2020; Neave and Maclennan 2020; Palummo et al. 2021). Specifically, the application of different diffusion modelling approaches to the clinopyroxene zoning pattern allows determining the duration of pre-eruptive processes which yield important information on the plumbing system evolution at active volcanoes (e.g., Morgan et al. 2004; Costa et al. 2013; Kilgour et al. 2014; Petrone et al. 2016, 2018, 2022; Flaherty et al. 2018; Di Stefano et al. 2020; Mangler et al. 2020; Pelullo et al. 2022). Recent investigations on the compositions and textures of zoned clinopyroxene, integrated with diffusion modelling, have elucidated how periodic magma replenishment, mixing, and intrusion events trigger volcanic activity at Stromboli and Mt. Etna (in South Italy), as well as in Mexican volcanic complexes (Petrone et al. 2018, 2022; Ubide and Kamber 2018; Di Stefano et al. 2020; Hughes et al. 2021; Mangler et al. 2022).

This approach is under-used on volcanic products that erupted in the Neapolitan area (Southern Italy) and, in general, a detailed reconstruction of pre-eruptive processes and their timescales are lacking for most of the volcanic events. Through diffusion chronometry, Morgan et al. (2004, 2006) estimated the residence times of crystals erupted during the 79 CE and 1944 eruptions of the Somma-Vesuvius volcanic complex. Similarly, diffusion modelling performed on clinopyroxene crystals yielded decadal times for the magmatic processes preceding the ~ 4.7 ka Agnano-Monte Spina eruption of the nearby Campi Flegrei caldera (Pelullo et al. 2022). However, these kinds of studies, particularly in conjunction with a systems diagram analysis of connectivity between different magmatic environments (e.g. Kahl et al. 2011, 2015), have never been applied to the Ischia island products. Therefore, the rationale of this work is to fill this gap through the application of such methodology to a recent eruption of that volcanic complex.

Ischia hosts a permanent population of about 60,000 people, which greatly increases during spring and summer and therefore the volcanic risk is extremely high. In fact, the last 10 ka is the reference time window for probabilistic volcanic hazard assessment at Ischia (Selva et al. 2019).

Based on these premises, in the present study, we performed high spatial resolution microanalysis of major and minor elements of chemically zoned and unzoned clinopyroxene crystals of the effusive Zaro eruption, which occurred at Ischia < 7 ka. The Zaro lava complex is made up of several trachytic lava flows hosting shoshonitic to trachytic enclaves. The textural, chemical and isotopic characteristics of the Zaro lavas suggest that refilling of a pre-existing, evolved magma reservoir and mingling/mixing processes occurred prior to the eruption (Pelullo et al. 2020). These features make the Zaro eruption an excellent case study to provide information on the plumbing system evolution, the pre-eruptive magma dynamics and the timescales of magmatic processes during the last 10 ka of the Ischia activity.

We have studied the zoning patterns of Fe–Mg in Zaro clinopyroxene crystals. In addition, the dynamical processes responsible for the patterns shown by the enclaves have been modelled through two-dimensional numerical simulations of physical mixing between the intruding shoshonitic magma and the host trachytic reservoir. These models reproduce the physical evolution of the interacting magmas and yield information on the timescale of the mingling process. We have combined results from numerical simulations with the compositional zoning in clinopyroxene and diffusion modelling. Our results shed light on the dynamics of magmatic processes that operated at different spatial and temporal scales in the Zaro plumbing system before the eruption. The complex interplay of various pre-eruptive processes plays a central role in setting the stage for critical factors that trigger an eruption. Therefore, a comprehensive understanding of the nature and temporal scales of pre-eruptive processes is crucial for accurate volcanic hazard assessment and for implementing effective risk mitigation strategies.

Geological setting

Ischia island

The Neapolitan area includes the three active volcanoes of Ischia, Somma-Vesuvius and Campi Flegrei caldera (Fig. 1).

This area has a population of about three million people and it would be exposed to severe volcanic and related hazards in the case of renewed volcanic activity (Orsi et al. 2003).

Ischia is an active volcanic field in the north-western corner of the Gulf of Naples (Fig. 1a). Its complex volcanic history, characterized by alternating constructive and destructive volcanic and volcano-tectonic phases, also including caldera-forming events and block resurgence (Fig. 1a), started > 150 ka and has been divided into different periods of both explosive and effusive activity, based on geochronological data along with volcanological and geochemical features of the emitted products (Fig. 1a; Poli et al. 1987; Vezzoli 1988; Civetta et al. 1991; Brown et al. 2008, 2014; Sbrana et al. 2018; Selva et al. 2019).

Volcanic activity in the last 10 ka has been strongly influenced by the resurgence mechanism. It is characterized by several effusive and explosive eruptions, which occurred mostly in the eastern sector of the island and culminated with the Arso eruption in 1302 AD (Vezzoli 1988; de Vita et al. 2010; Marotta and de Vita 2014). During the last 10 ka, the magmatic system has been characterized by the arrival of geochemically and isotopically distinct magmas that show evidence of crustal contamination and magma mixing (Civetta et al. 1991; Piochi et al. 1999; D'Antonio et al. 2013; Iovine et al. 2017). Several studies (Civetta et al. 1991; Orsi et al. 1996; D'Antonio et al. 2013; Moretti et al. 2013; Casalini et al. 2017; Marotta et al. 2022) proposed that the magmatic system of Ischia is made up of a deep and poorly evolved magma reservoir, where mantle-derived magmas stagnate and are interconnected with shallow reservoirs hosting more-evolved magma batches.

The present state of activity of Ischia volcano is testified by historical eruptions (de Vita et al. 2010), historical and present-day seismicity (e.g. Casamicciola earthquakes in 1881, 1883 and 2017; Cubellis et al. 1995; Nappi et al. 2018, 2021; De Novellis et al. 2018; Trasatti et al. 2019; Giudicepietro et al. 2021 and references therein), and intense hydrothermal and fumarolic activity (Chiodini et al. 2004; Fabbrocino et al. 2022).

During the last 10 ka, only a few events occurred outside the eastern sector of the island, along the caldera rims. In particular, the Zaro eruption occurred at the intersection between regional faults and volcano-tectonic structures reactivated during both caldera formation and resurgence (de Vita et al. 2010). Therefore, the Zaro eruption constitutes a unique case study to provide information on the relationships between evolved magmas, stagnating at shallow depth, and less evolved melts directly ascending from the deep magmatic reservoir in the most recent period of activity.

Petrological features of the Zaro lava complex

The Zaro eruption originated at 6.6 ± 2.2 (Vezzoli 1988) ka in the north-western corner of Ischia (Fig. 1a) from NE-SW trending eruptive fractures (Fig. 1b; Vezzoli et al. 2009; de Vita et al. 2010; Sbrana et al. 2018) and produced a ~ 0.1 km^3 lava complex. It is composed of stacked asymmetric domes, scoria cones and viscous lava flows, affected by NW–SE oriented strike-slip faults (Vezzoli et al. 2009). Pelullo et al. (2020) provided a detailed petrographic, chemical, and isotopic characterization of the Zaro lava complex, summarized below.

The main *lava* flows are porphyritic trachytic rocks, with a ~ 50% crystals content. Phenocrysts of sanidine (up to 1 cm in size, $An_{15-4}Ab_{65-34}Or_{62-20}$) together with minor phlogopite, clinopyroxene, plagioclase and Ti-magnetite are immersed in a microcrystalline groundmass, made up of the same mineral phases, plus apatite. The lava hosts three chemically different lithotypes in the form of enclaves (Fig. 1c):

- The *felsic enclaves* are rounded and weakly flattened, centimeter- to decimeter-large trachytic blocks embedded in the lava. They show the same crystal assemblage and trachytic texture as the host lava, but have a higher amount of glass in the groundmass. Some felsic enclaves host rounded decimeter-sized lava fragments (Fig. 1d). Lavas and felsic enclaves show a small range of isotopic composition, for both whole rocks and minerals, having $^{87}Sr/^{86}Sr = 0.70607–0.70615$ and $^{143}Nd/^{144}Nd = 0.51255–0.51256$.
- The *mafic enclaves* consist of dark gray/blackish, vesicular, centimeter-to decimeter-sized shoshonitic lava fragments, embedded in both lava and felsic enclaves. These enclaves are ellipsoidal and have a sharp contact with host rocks, often with cuspate borders (Fig. 1e). Mafic enclaves are porphyritic with phenocrysts and microphenocrysts of olivine (Fo_{87-71}), clinopyroxene, plagioclase ($An_{86-70}Ab_{24-13}Or_{6-1}$), sanidine ($Ab_{55-39}Or_{56-38}An_{8-4}$) and Ti-magnetite. The enclaves exhibit segregation vesicles, variable crystal size distribution, chilled margins at the contact with the host trachyte, disruption of the boundary due to infiltration and engulfment of, or inter-fingering with, the host trachyte. Their $^{143}Nd/^{144}Nd$ ratios are remarkably high (0.51268–0.51269) whereas their $^{87}Sr/^{86}Sr$ (0.70495–0.70500) are among the lowest values detected in rocks of the Neapolitan area. Olivines from mafic enclaves exhibit very low Sr isotopic compositions (0.70485–0.70493), whereas clinopyroxenes vary in a wider range (from 0.70560 to 0.70623). Feldspars have the highest and most homogeneous $^{87}Sr/^{86}Sr$ ratios (0.70602–0.70623), defining the same range as the lava and felsic enclave rocks and minerals (feldspars and clinopyroxenes).
- The *hybrid enclave* displays mineralogical, chemical, and isotopic characteristics that are intermediate between those of the mafic enclaves and the felsic lavas. The crystal assemblage is made up of phenocrysts of plagioclase ($An_{82-24}Ab_{61-17}Or_{14-2}$), sanidine ($An_{4-2}Ab_{61-39}Or_{57-37}$),

clinopyroxene, olivine ($Fo_{86–72}$) that hosts Cr-Al-spinel, and phlogopite in a holocrystalline groundmass, composed of sanidine and subordinate plagioclase, clinopyroxene, Ti-magnetite and ilmenite. The hybrid enclave composition straddles the boundary between latite and trachyte; it shows isotopic signature ($^{87}Sr/^{86}Sr = 0.70584$ and $^{143}Nd/^{144}Nd = 0.51258$) intermediate between those of the Zaro felsic and mafic rocks.

Methods

Samples preparation

Clinopyroxene crystals have been picked from several samples representative of the four lithotypes of the lava complex (Fig. 1b; Online Resource 1). Samples ZR3A, ZR1A and M1 belong to the lava, samples ZR3B and ZR1B belong to the felsic enclaves, sample M6C belongs to the hybrid enclave and samples ZR3C, ZR1C and M4C belong to the mafic enclaves. Samples from the same lithotype collected in different sites (Fig. 1b) show similar chemical and textural characteristics (Pelullo et al. 2020). The selected lava samples were gently crushed to lapilli-size grains through a jaw crusher. About 500 g of crushed rock for each sample were sieved using a stack of sieves with meshes diameter ranging from 1 mm to 250 µm. From the sieved aliquots, about 100 clinopyroxene crystals for each lithotype were selected and observed under both binocular and scanning-electron microscope, before performing compositional analyses. Crystals were glued in epoxy resin, oriented along the maximum axis (presumably the c-axis), and polished to obtain detailed in-situ analytical data.

Electron micro probe analysis (EMPA) data

The major and minor elements (Si, Ti, Al, Fe, Mg, Mn, Ca, Na, K, Ni and Cr) concentrations were obtained on 79 clinopyroxene crystals (Online Resource 1) embedded in carbon-coated resin mounts. 59 analytical spots have been acquired on 29 unzoned crystals and further 30 on 14 patchy zoned crystals. Moreover, chemical composition was acquired along analytical traverses on 35 zoned clinopyroxenes: 9 crystals from mafic enclaves, 10 crystals from the hybrid enclave, 3 crystals from felsic enclaves and 13 crystals from the host lava. A compositional traverse has been obtained also on one unzoned crystal from the lava. Mineral microanalysis was carried out along with:

- core-to-rim or rim-to-rim traverses, varying from 80 to 800 µm, with a spacing between individual points varying in the range 5–70 µm;
- one- or more- detailed traverses, crosscutting crystal zones boundaries, varying from 6 to 60 µm, with a spacing between individual points varying in the range 1–2.5 µm.

Crystals were traversed using spots with variable beam diameter of 2.5 and 5 µm, depending on the transect length. The 5 µm beam size has been set for the long core-to-rim and rim-to-rim profiles mostly used to characterize the zoning pattern of the Zaro clinopyroxenes. The 2.5 µm beam size has been set for the detailed profiles mostly used for thermobarometry and diffusion modelling. Two transects, perpendicular to each other, were acquired in some of the crystals. The data were obtained at the HP-HT Laboratory of Experimental Volcanology and Geophysics of the Istituto Nazionale di Geofisica e Vulcanologia in Rome (Italy), with a Jeol-JXA8200 electron microprobe equipped with five wavelength dispersive X-ray spectrometers, using an accelerating voltage of 15 kV. The electron beam current was set at 7.5 nA. Elemental counting times were 10 s on the peak and 5 s on each of two background positions. Corrections for inter-elemental effects were made using a ZAF routine. Calibration used a range of standards from Micro-Analysis Consultants (MAC; http://www.macstandards.co.uk): albite (Si-PET, Al-TAP, Na-TAP), forsterite (Mg-TAP), augite (Fe-LIF), apatite (Ca-PET), orthoclase (K-PET), rutile (Ti-PET), and rhodonite (Mn-LIF). Smithsonian augite (Jarosewich et al. 1980) and MAC augite were used for quality control and for the calculation of accuracy and precision. Accuracy was within 1–5% except for elements with abundances below 1 wt%, for which accuracy was 5–10%. Precision was typically 1–5% for all analyzed elements.

Approaches for the study of the zoning pattern

In this study, we use the term "zone" to describe a spatial region of a crystal characterized by a specific brightness in a BSE image and a homogeneous composition (or at most a very weak variation in composition). Minerals can be characterized by two or more zones with constant composition (plateau). A zone with a constant composition in a crystal indicates a growth under a constant set of intensive thermodynamic variables (P, T, bulk composition including fluid chemistry expressed through the fugacity of different species); the occurrence of two or more such plateau compositions in a crystal implies that one or more of these thermodynamic variables changed in the course of the crystal growth (e.g. Costa et al. 2008; Kahl et al. 2015). The set of thermodynamic intensive variables associated with a zone constitutes a Magmatic Environment (ME, see Kahl et al. 2015 for a detailed explanation). Significantly, a ME is an abstract entity and it is distinct from a magmatic reservoir with physical boundaries (i.e. two distinct MEs may

be two separate physical reservoirs, or different parts of a heterogeneous magma chamber). Since the composition of each zone is associated with a specific set of variables (i.e. a specific ME), sequential zoning represents crystal growth at different stable conditions, with residence times in each ME long enough to be recorded, but short enough not to erase a compositional gradient among zones by diffusional equilibration (e.g., Kahl et al. 2011, 2013; Dohmen et al. 2017). By quantifying the different types of zoning among the different MEs, the chemical information recorded in Zaro clinopyroxenes has been decoded, allowing the reconstruction of the evolutionary history of the magma(s) that fed the plumbing system. The extent of diffusion between different zones, or the lack thereof, is a measure of the residence times of a crystal in different MEs.

Magma mingling dynamics

The complex interactions among compositionally different magmas within the Zaro plumbing system have been modelled to unravel the dynamical processes that produced the patterns observed both in the field and in the analyzed samples. We used MagmaFOAM (Brogi et al. 2022), a computational fluid dynamics framework specifically suited for tackling volcanic systems, to simulate plumbing system magmatic processes preceding the Zaro eruption. As a first approximation, we only included two magmatic end-member compositions: an evolved trachyte and an intruding shoshonite. The simulation setup is described in Fig. 2 and a detailed description is given in Online Resource 2. A vertically elongated magmatic reservoir containing a trachytic magma is invaded by the shoshonitic end-member (Fig. 2).

The vertically elongated reservoir geometry (0.1 km × 1 km) has been chosen based on the geophysical evidences of dykes that intruded tectonic and volcano-tectonic structures in the Ischia eastern and northwestern sectors, feeding the past 10 ka volcanic activity (de Vita et al. 2010; Marotta et al. 2022). Dimensions have been chosen considering the estimated total erupted volume of ~ 0.1 km^3 of the Zaro eruption (Vezzoli et al. 2009). The bottom part of the reservoir contains shoshonitic melt that is roughly 5 vol%, as observed in the erupted products (Pelullo et al. 2020).

Since the reservoir is relatively small, corresponding to the erupted volume of the Zaro lava complex, the physical properties of magmas (density, viscosity) are not expected to vary too much as a consequence of volatile exsolution within the system, and we assume they are constant throughout the simulation. We have used two setups, one considering a low-viscosity, crystal-free trachytic melt and one with a high-viscosity trachytic melt which contains 50% in volume of crystals, as observed in the erupted products (Online Resource 2). The intruding shoshonite has a slightly larger volatile content and is therefore buoyant with respect to the resident trachytic end-member. The simulation is bi-dimensional, but the overall features of magmatic interaction are expected to be preserved as in full three-dimensional configurations (Garg and Papale 2022).

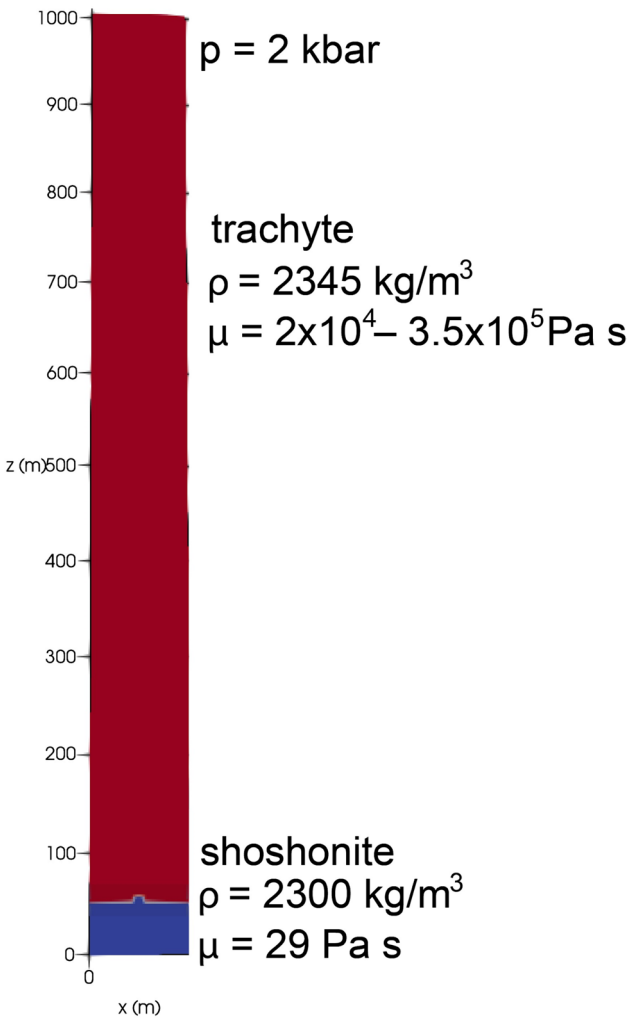

Fig. 2 Setup for the simulations of magmatic interactions in the Zaro plumbing system. The small 2D vertically elongated reservoir contains trachyte (in red) and is intruded by shoshonite (in blue) from the bottom

Results

The Zaro clinopyroxene

Zaro clinopyroxene occurs as visually (in backscattered–BSE images) zoned or unzoned crystals. Different kinds of zoning have been recognized. The unzoned clinopyroxenes (Fig. 3a) make up the 58–78% of the whole

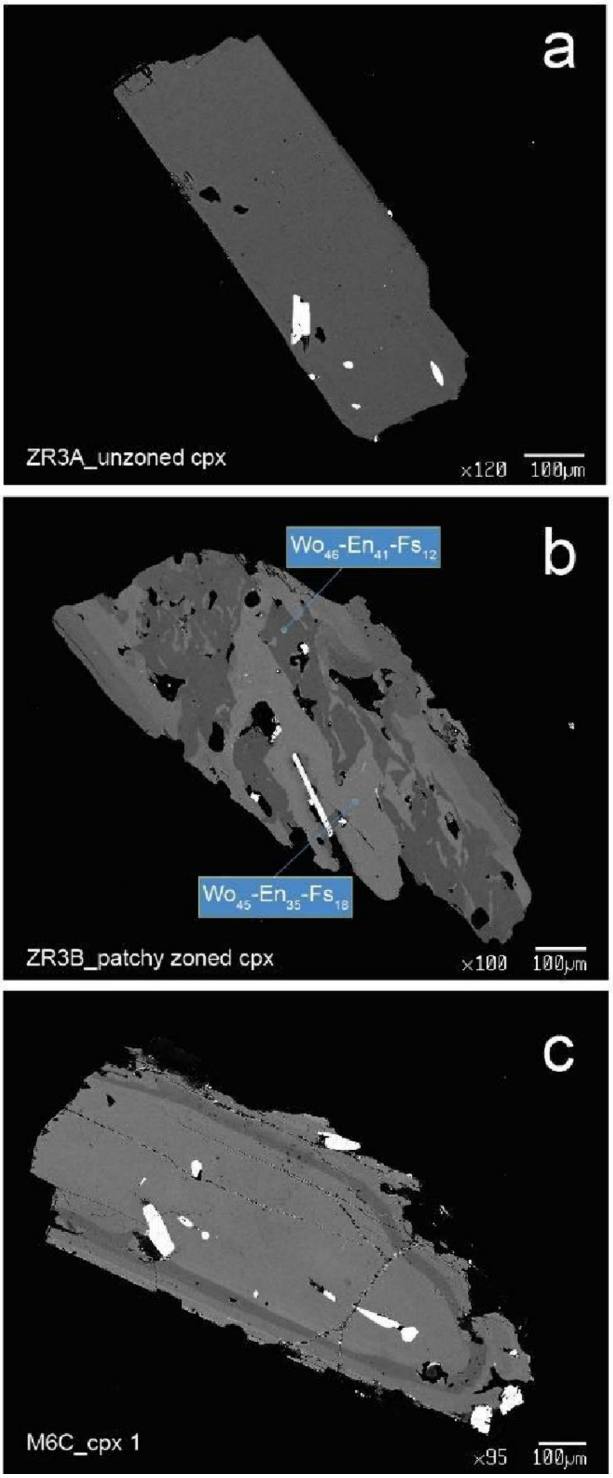

Fig. 3 BSE images of Zaro clinopyroxenes showing unzoned and different kinds of zoned crystals: **a** unzoned clinopyroxene crystal from lava; **b** patchy zoning in a clinopyroxene crystal from a felsic enclave, characterized by different compositions in the different colored areas; **c** concentric zoning in a clinopyroxene crystal from the hybrid enclave; white minerals are opaques

Table 1 Percentages of unzoned and different kinds of zoned clinopyroxenes from the Zaro lithotypes

Lithotype	Unzoned crystals (%)	Zoned crystals	
		Patchy zoning (%)	Regular zoning (%)
Lava	73	14	13
Felsic enclaves	78	19	3
Hybrid enclave	63	26	11
Mafic enclaves	58	33	9

investigated crystals, depending on the different Zaro lithotypes (Table 1).

Zoned crystals can be divided into two main groups depending on the texture of the zoning: patchy zoned crystals, characterized by irregular areas, with different color tones in BSE images, having different compositions, represent ~ 70% of the zoned clinopyroxenes (Fig. 3b, c). The remaining ~ 30% show regular texture mostly characterized by concentric zones (Fig. 3d). Among the latter, some crystals also show patchy zoned or resorbed cores (Online Resource 1). For the regularly zoned crystals, ''mantle" refers to the visually distinguishable area between the core and the rim.

Most clinopyroxenes from the different Zaro lithotypes are diopsidic/Fe-diopsidic (Fig. 4) in composition, with Mg# [molar $Mg^{2+}/(Mg^{2+}+Fe_{tot})\times100$] ranging from 86 to 57 (Fig. 5).

Clinopyroxenes from lava ($Wo_{52-44}En_{36-30}Fs_{25-13}$; Fig. 4a) and felsic enclaves ($Wo_{48-45}En_{41-34}Fs_{19-12}$; Fig. 4a) exhibit Mg# ranging from 77 to 57 and from 77 to 66, respectively (Fig. 5). The composition of clinopyroxenes from the hybrid enclave is $Wo_{47-44}En_{45-33}Fs_{22-8}$ (Fig. 4b) with Mg# ranging from 84 to 60. Clinopyroxenes from mafic enclaves ($Wo_{47-46}En_{45-32}Fs_{22-8}$; Fig. 4b) have Mg# ranging from 86 to 62.

Part of clinopyroxenes from mafic and hybrid enclaves show substantial differences in the Mg, Fe, Al, Ti, Cr, Mn and Al^{VI} contents, with respect to those of the lava and felsic enclaves. Indeed, clinopyroxenes from mafic and hybrid enclaves have larger variations and higher Mg# and Al_2O_3, TiO_2, and Cr_2O_3 contents compared to those from felsic rocks (Fig. 5a–c): in clinopyroxenes from mafic and hybrid enclaves, the Cr_2O_3 content ranges between 0.9 and < 0.1 wt%, whereas in clinopyroxenes from lava and felsic enclaves, Cr_2O_3 ranges between 0.2 and < 0.1 wt%; in clinopyroxenes from mafic and hybrid enclaves, the ranges of TiO_2 and Al_2O_3 contents (3.2–0.2 wt% and 7.9–1.1 wt%, respectively) are substantially higher than those (1.8–0.4 wt% and 4.3–1.1 wt%, respectively) of clinopyroxenes from evolved lithotypes. Moreover, higher Al^{VI} contents of

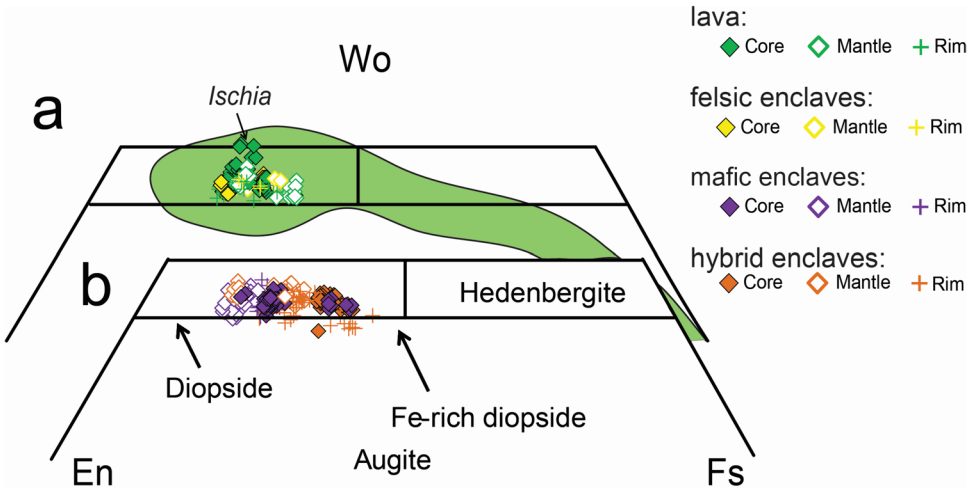

Fig. 4 Di-Hd-En-Fs classification diagram for the Zaro clinopyroxenes from **a** the trachytic lithotypes and **b** the poorly evolved enclaves (data on Ischia clinopyroxene from literature, in the green field, are from D'Antonio et al. 2013, 2021; Melluso et al. 2014; Iovine et al. 2017); "mantle" refers to the visually distinguishable area between the core and the rim; Wo: wollastonite, En: enstatite, Fs: ferrosilite

clinopyroxenes from mafic and hybrid enclaves suggest crystallization at higher pressure conditions, compared to those from felsic rocks (Fig. 5d; Wass 1979; Seyler and Bonatti 1994; Putirka et al. 1996; Wang et al. 2021). However, in general, none of the analyzed clinopyroxene seems to have formed at a very high pressure, a common feature at Ischia (Melluso et al. 2014).

Additional to the diopsidic/Fe-diopsidic compositions, omphacite and aegirin-augite components were detected at the rims of three clinopyroxene crystals from the lava and two crystals from the hybrid enclave. These Na-rich components (with Na_2O up to 2.1 wt%; Fig. 5e) show significantly lower Mg# (from 57 to 48) compared to those of all the other clinopyroxenes. Their CaO and FeO (and also Fe^{3+}) contents are respectively lower and higher than those of the diopsidic clinopyroxenes (Fig. 5f, g). They also show lower Al_2O_3 and higher MnO contents (Fig. 5a, h) than the other clinopyroxenes. Aegirine-rich pyroxene, which is the most reliable indicator of the transition to peralkaline conditions, is found in nearly all trachytic rocks of all cycles of the Ischia activity (Melluso et al. 2014).

Clinopyroxene compositional populations

A detailed analysis of the whole chemical variation of the Zaro clinopyroxenes has revealed a polymodal distribution (well evident in the regularly zoned crystals), made up of three different compositional populations (Fig. 6): a population with high Mg#, in the range 86–80, is hereafter named ME0; the ME1 population has Mg# between 79 and 70; the ME2 population is characterized by low Mg#, in the range 69–58.

The unzoned clinopyroxene crystals show a homogeneous composition, which corresponds to ME1. Crystals with patchy zoning show narrow compositional ranges: ME2 and ME1 occur in clinopyroxenes from evolved rocks and ME1 and ME0 in clinopyroxenes from less evolved rocks (Fig. 6b). The three compositional populations are distributed in the different zones of the regularly zoned crystals as summarized in Fig. 7.

In summary, ME1 is the dominant environment, occurring in all the unzoned clinopyroxenes and in most rims and many cores of regularly zoned clinopyroxenes from the four lithotypes. ME0 is restricted to mafic and hybrid enclaves, in particular in the mantles. ME2 is dominant in the evolved lavas and hybrid enclave and, to a lesser extent, in the mafic enclaves, in particular in the core of crystals.

Besides these main populations, five crystal rims characterized by Mg# in the range 57–48 pertain to the Na-rich (aegirin-augitic) clinopyroxenes.

Clinopyroxene zoning pattern

The pattern of the regularly zoned clinopyroxenes (Fig. 3d) consists of two or more zones showing a constant composition separated by either sharp or gradual boundaries (Fig. 8).

The terms "sharp" or "gradual" are used here in the context of the spatial resolution chosen for the electron microprobe analyses of concentration profiles. It is important to note that a "sharp" profile might reveal diffusive boundaries when studied with an analytical instrument with a higher spatial resolution (e.g. analytical transmission electron microscopy).

Reverse and normal zoning are defined by Mg# increasing and decreasing, respectively, from the core toward the rim of a crystal. We have defined different zoning types based on the connectivity between different MEs, as follows:

Type I clinopyroxenes involve variations between ME1 and ME2 (Fig. 8a). Based on the Mg# variation, we further distinguish *Type IA* crystals characterized by reverse zoning, *Type IB* crystals showing reverse-to-normal zon-

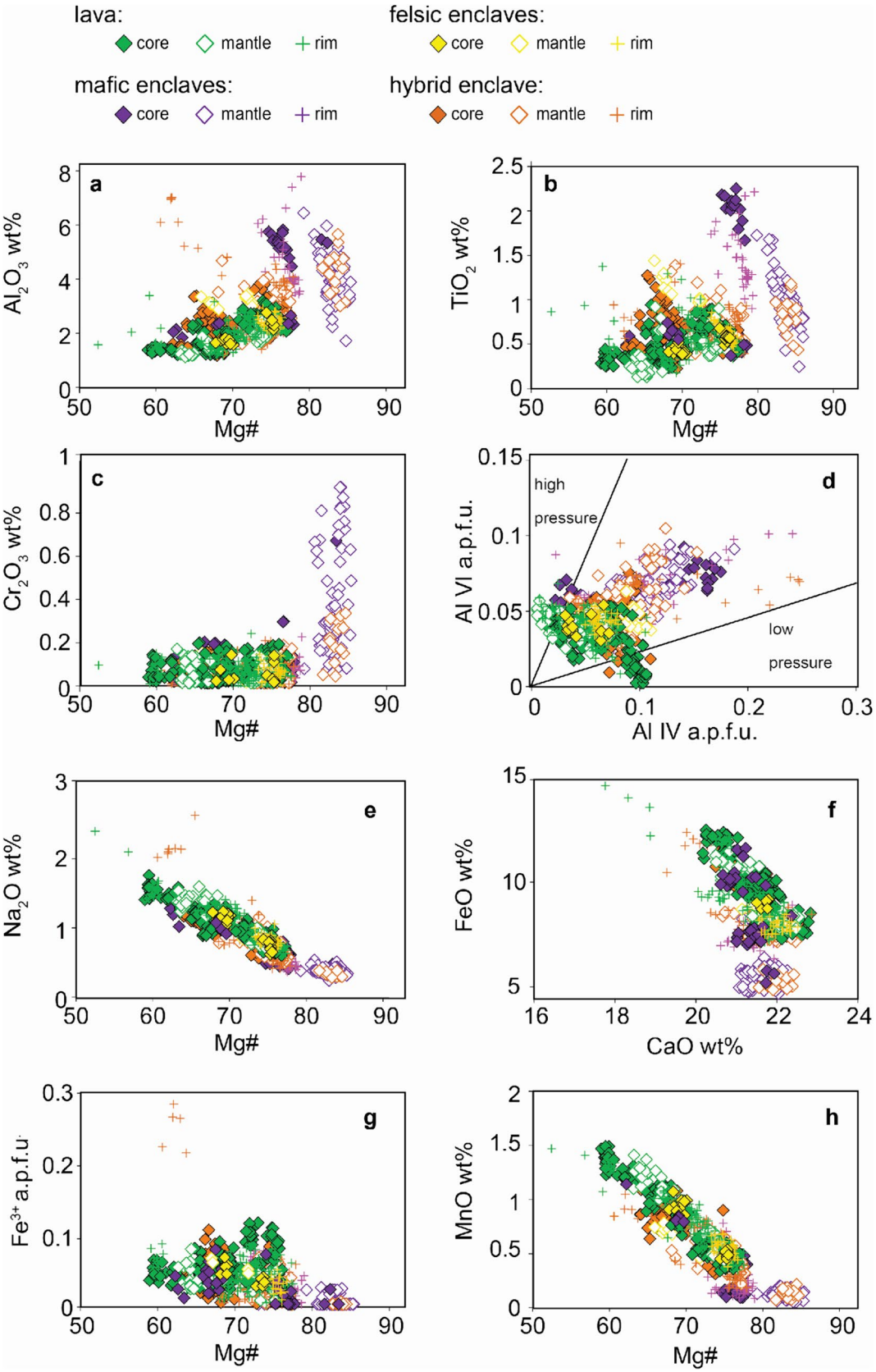

Fig. 5 Chemical variation diagrams showing differences among clinopyroxenes of the Zaro rocks; Al^{IV} a.p.f.u. = 2-Si a.p.f.u.; Al^{VI} a.p.f.u. = Al_{tot}-$Al.^{IV}$ a.p.f.u. In **d**, fields from Aoki and Shiba (1973)

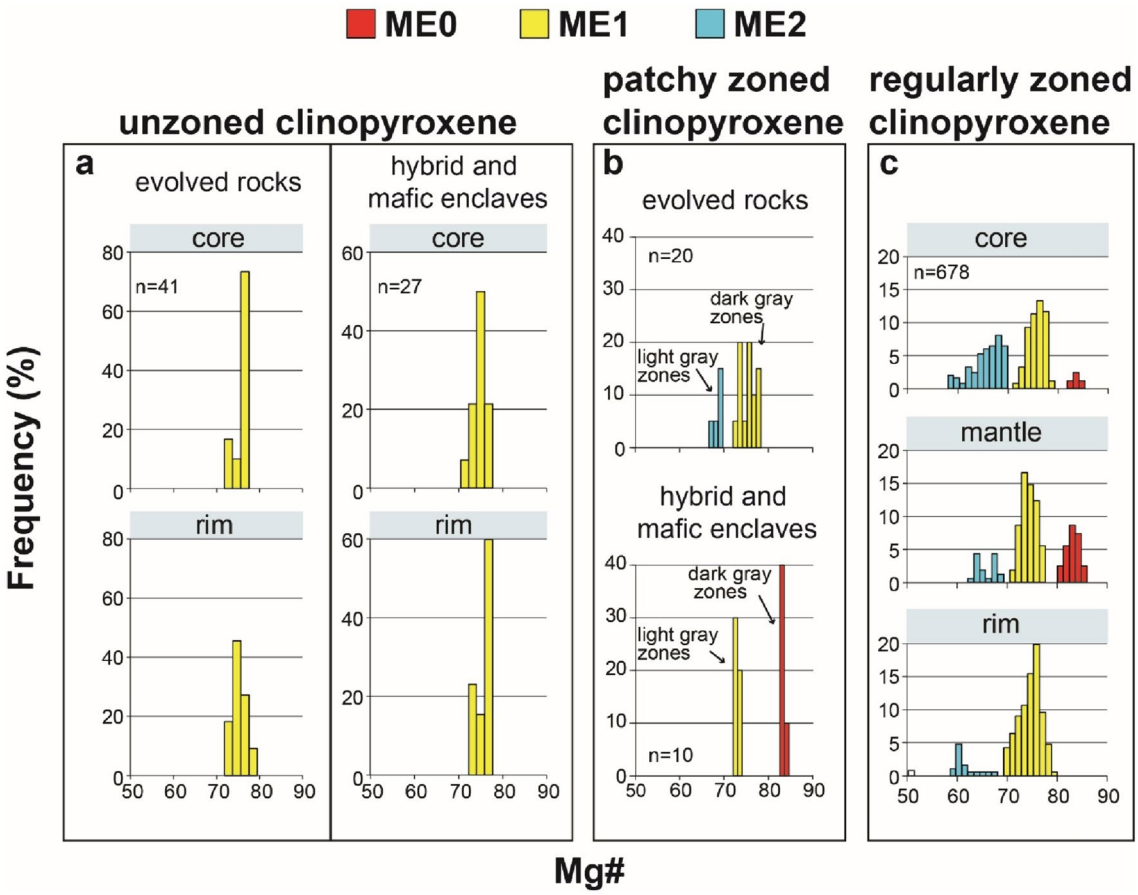

Fig. 6 **a** Mg# frequency histograms of core and rim of unzoned clinopyroxene crystals; **b** Mg# frequency histograms of patchy zoned clinopyroxene crystals. **c** Mg# frequency histograms of core, mantle and rim of the regularly zoned clinopyroxenes; these allow different populations to be identified

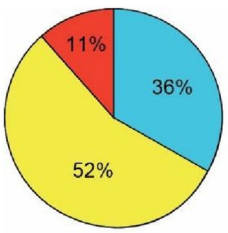

Population / Lithotype	ME0 Mg#=86–79			ME1 Mg#=78–70			ME2 Mg#=70–58		
	c	m	r	c	m	r	c	m	r
lava				5%	3%	8%	8%	7%	5%
felsic enclaves				1%		3%	2%	1%	
hybrid enclave		1%		5%	7%	7%	6%	1%	1%
mafic enclaves	1%	9%		5%	3%	7%	2%		4%
% tot.	**1%**	**10%**		**16%**	**13%**	**25%**	**17%**	**10%**	**9%**
	11%			**52%**			**36%**		

Fig. 7 The pie chart represents the percentage of the compositional populations in the whole set of the regularly zoned crystals; the colored table reports, for each lithotype, the frequency of occurrence of a compositional population in a zone (core, mantle or rim) in a total of 35 analyzed zoned clinopyroxene crystals of the Zaro lava complex; c = core; m = mantle; r = rim; percentages have been calculated considering 35 cores and rims (corresponding to the total number of analyzed regularly zoned crystals) and 17 mantles (due to the occurrence of some crystals displaying complex zoning)

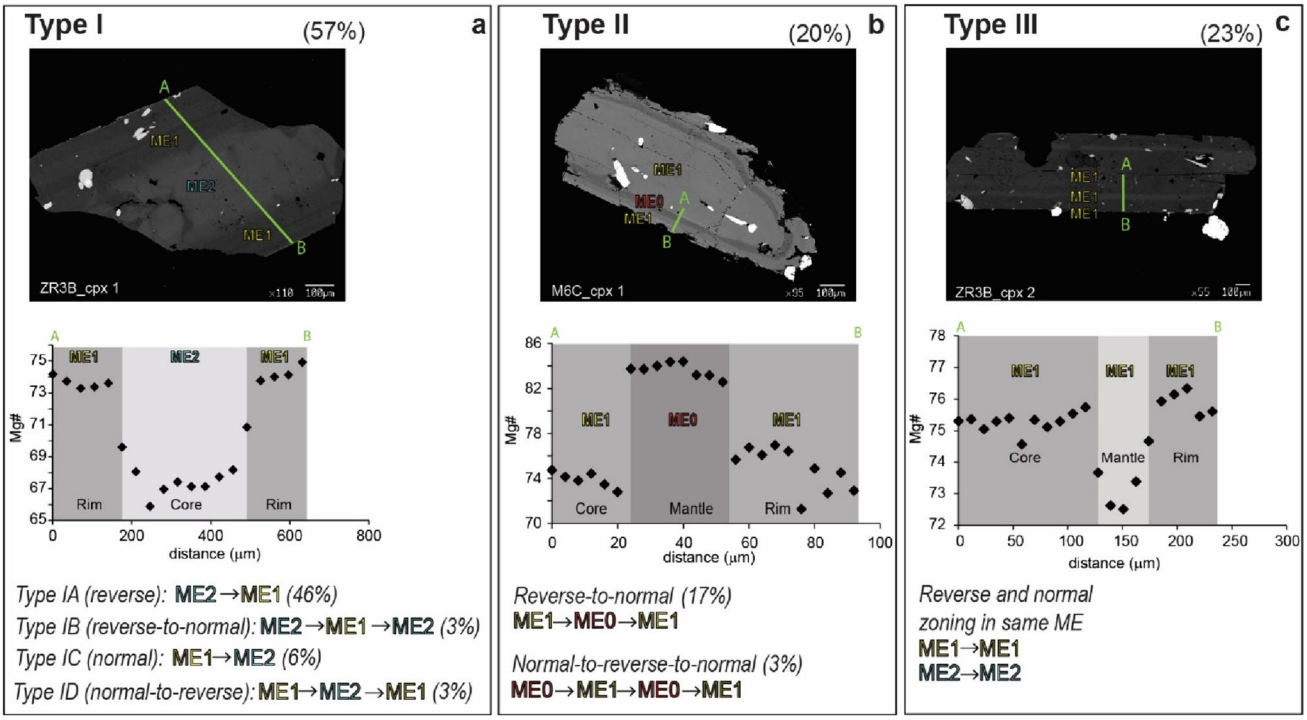

Fig. 8 BSE images and types of zonation for the Zaro clinopyroxenes; black diamonds are points measured along the crystal traverses (indicated by green lines in the BSE images) from core-to-rim or rim-to-rim [Mg# = molar $Mg^{2+}/(Mg^{2+} + Fe_{tot})$]. The numbers in parentheses indicate the percentage of zoned clinopyroxenes exhibiting such a pattern

ing, *Type IC* characterized by normal zoning and *Type ID* crystals showing normal-to-reverse zoning (Fig. 8a). Type II clinopyroxenes involve variations between ME0 and ME1 (Fig. 8b).

Type III crystals show zoning within the same ME (Fig. 8c), and may occur in any ME. Some of these variations also occur at the zone boundaries of Types I crystals.

Type I is the most common (~57%) zoning type. An important observation is that 30 out of 35 zoned clinopyroxenes are characterized by reversely zoned cores.

Sequential growth recorded in the Zaro clinopyroxenes

The core-to-rim compositional (e.g., Mg#) variations recorded in the Zaro clinopyroxene zoning patterns can be used to track the sequential growth of crystals at distinct crystallization conditions (ME). A systems connectivity diagram (Fig. 9) illustrates the connections between the different MEs as recorded by zoning in clinopyroxenes in different rock compositions.

Since each line indicates the composition of a crystal from core to rim in terms of MEs, the diagram also represents the relative abundance of each kind of connection. In spite of the diversity of zoning types, certain patterns in the pathways recorded by the compositional zoning emerge from this analysis. First, most pathways (all Type II and most Types I and III zoning) end in ME1, which represents the dominant rim composition of crystals from all lithotypes found in Zaro (e.g., Figs. 6c, 7). It is worth recalling here that 70% of the clinopyroxene crystals found in the Zaro rocks have ME1 compositions and are unzoned.

Figure 9 also shows the frequency of occurrence of the zoning types in the different lithotypes. In fact, substantial differences occur between the various Zaro lithotypes. For example, Type II zoning is restricted to the mafic and hybrid enclaves. On the other hand, Type I zoning is found in all lithotypes and Type III zoning occurs in the trachytic lavas and the hybrid enclave.

P–T crystallization conditions of Zaro clinopyroxenes

In order to investigate the crystallization conditions of the Zaro clinopyroxenes, clinopyroxene-liquid thermometers and barometers specific for alkaline magmas (Masotta et al. 2013) have been used. For the melt-clinopyroxene pairs, we considered in equilibrium only those with $^{Fe/Mg}Kd_{cpx\text{-}liq} = 0.27 \pm 0.03$ (Grove and Bryan 1983; Putirka et al. 2003; Mollo et al. 2013; Fig. 10a).

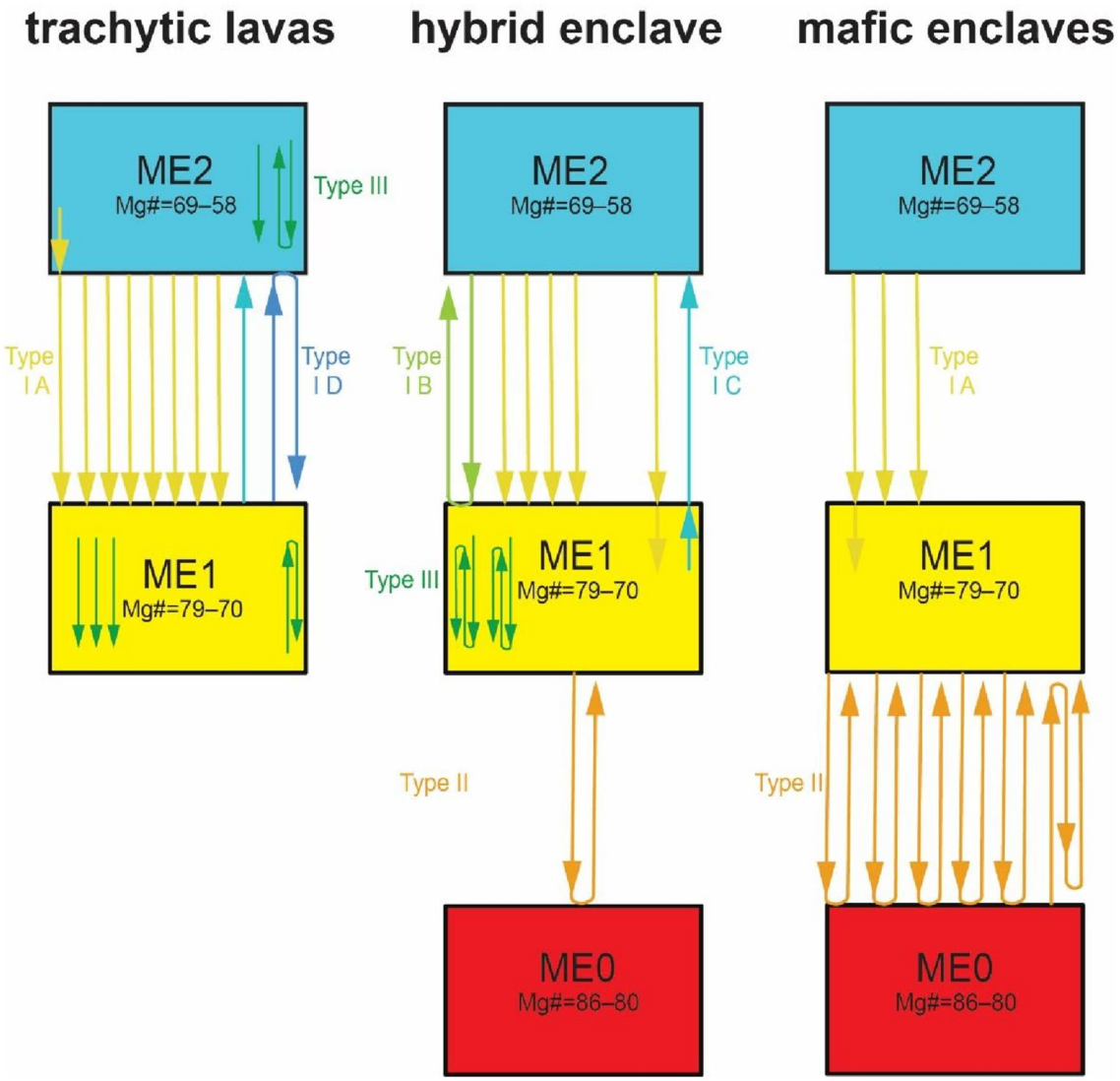

Fig. 9 System analysis of the zoning patterns of Zaro clinopyroxene crystals. Each box represents a ME, hence, a set of conditions that define a specific compositional population. A single arrow represents the passageway of a crystal from an environment to a different one, characterized by a different set of conditions, e.g., by higher temperature. The lines inside the box represent compositional steps inside the same ME (i.e. from Mg# 75 to Mg# 72 in Fig. 8c; the meaning of these passageways is addressed in the Discussion section). Each line indicates the composition of a crystal from core to rim: in other words, each different colored line represents a zoning type. The whole set of lines shows the dominant passageways of crystals (or a magma in which the crystal was growing) in different environments

Results indicate that some ME0 clinopyroxenes (Mg# > 82) are in equilibrium with the composition of the mafic enclaves (Fig. 10a). The ME0 clinopyroxenes from the hybrid enclave (Mg# > 79), on the other hand, are out of the equilibrium field, whereas some clinopyroxenes from the hybrid enclave with ME1 composition are in equilibrium with their host rock (Fig. 10a). Several clinopyroxene crystals from trachytic lithotypes (lava and felsic enclaves) are in equilibrium with their host rocks (Fig. 10a). Some of the ME1 clinopyroxenes with Mg# in the range 73–70 are in equilibrium with trachytic rocks (lava and felsic enclaves) with Mg# in the range 39–37. ME2 clinopyroxenes with Mg# in the range 69–63 are in equilibrium with trachytic rocks having Mg# in the range 36–33. The estimated P–T conditions (Fig. 10b) are summarized in Table 2.

Diffusion modelling for the Zaro clinopyroxenes

Diffusion modelling applied to the clinopyroxene zoning pattern can provide information on the timescale of the magmatic processes that occurred in the Zaro plumbing system. The zones with constant composition found in most profiles can be used to infer the initial profile shapes before diffusive modification, where it occurred.

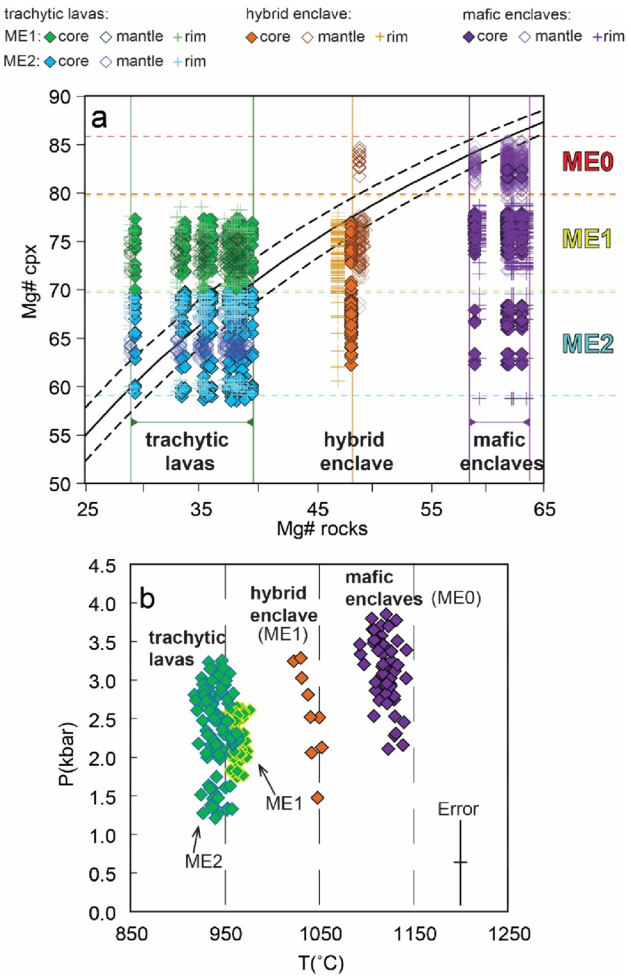

Fig. 10 **a** Test of equilibrium for the Zaro clinopyroxene: Fe–Mg partitioning between clinopyroxene and host rock ($^{Fe/Mg}Kd_{cpx\text{-}liq} = 0.27 \pm 0.03$; Grove and Bryan 1983; Putirka et al. 2003; Mollo et al. 2013); continuous line is $^{Fe/Mg}Kd_{Clinopyroxene\text{-}liq} = 0.27$; dotted lines = ± 0.03; gm: groundmass; **b** output temperatures and pressure estimates for the different couples obtained by the clinopyroxene-liquid thermometers (equation Talk2012) and barometers (equation Palk2012) specific for alkaline magmas (Masotta et al. 2013). Data on Zaro rock compositions are from Pelullo et al. (2020)

The initial conditions depend on the characteristics of the concentration profile shapes and, hence, two different approaches for modelling have been used. Some crystals are characterized by sharp gradients between zones with little evidence of diffusive modification of the growth zoning ("sharp" within the resolution of the EMPA analyses employed in this study; see definition of "sharp" above). These profiles have been modelled by method I, through which we calculated the relaxation of growth zoning timescales (e.g., Chakraborty and Ganguly 1991; Trepmann et al. 2004; Pelullo et al. 2022). This method allows to infer the possible uppermost limit of time that crystals may have spent in a ME at a given temperature without substantial diffusive modification of the profiles. The remaining profiles show diffusive gradients and these have been modelled through method II, by fitting the observed profiles. This approach yields durations of residence of the crystals in a ME.

For both methods, the diffusion equation

$$\frac{dC}{dt} = \frac{d}{dx}\left(D(t)\frac{d}{dx}\right) \quad (1)$$

has been solved to obtain t (time). The diffusion coefficient based on Fe–Mg interdiffusion rates in clinopyroxene obtained by Müller et al. (2013) has been calculated through:

$$D^{Fe-Mg} = 2.77 \pm 4.27 \times 10^{-7} exp\left(\frac{-320.7 \pm \frac{16kJ}{mol}}{RT}\right)\frac{m^2}{s} \quad (2)$$

where R is the gas constant and T is the temperature in Kelvin.

Temperatures for modelling a particular zoning profile were chosen according to the mean temperature at which the outer zone in a model (i.e. the mantle, for core-mantle models and the rim for core-rim or mantle-rim models) formed, according to the equilibrium and the results of thermometry (Fig. 10, Table 2). Accordingly, the following temperatures were used in Eq. (2) to obtain diffusion coefficients for modelling: ME1 rims of Type I and Type II crystals of the mafic and hybrid enclave: 1038 °C; ME1 mantles and rims of Type I and Type III clinopyroxenes from the trachytes: 962 °C. ME2 mantles and rims of Type IC crystals: 930 °C (Table 2).

In method I, the measured profiles are used as the initial profiles and forward modelling was carried out to obtain profiles that deviated perceptibly from the measured profiles within the resolution of measurement. As these

Table 2 Temperature and pressure crystallization conditions of clinopyroxenes from the different lithotypes of the Zaro lava complex

Lithotype	Cpx composition	T(°C) range	T(°C) average value—s.d	P (kbar) range	P (kbar) average value—s.d
Mafic enclaves	ME0	1140–1092	1120 ± 11	3.8–2.1	3.1 ± 0.4
Hybrid enclave	ME1	1052–1022	1038 ± 9	3.3–1.5	3 ± 0.6
Trachytic lavas	ME1	976–947	962 ± 6	2.7–1.7	2 ± 0.2
Trachytic lavas	ME2	963–917	930 ± 10	3.3–1.2	2 ± 0.5

zoning patterns show no diffusive modification, timescales on which such perceptible deviation from the starting profile occurs represent the upper limit of time that the crystal may have spent in the relevant ME (e.g. at 1038 °C).

In method II, on the other hand, it is necessary to define the shape of the initial profiles and then model its diffusive modification. In this case, initial conditions are defined by the homogeneous measured concentrations that define the plateau representing the ME for that zone (e.g. core, mantle or rim) with a step discontinuity between adjacent zones. Diffusion is allowed to proceed from such initial conditions until the calculated profiles match the measured ones, with the time required for such a match representing the residence time in the ME corresponding to the outer zone. Profiles modelled with both methods and detailed information are shown in Online Resource 3.

In both approaches, timescale information has been extracted only from crystals showing concentration profiles suitable for diffusion modelling, e.g., no profiles, in which the resolution is low (spacing between analytic points is large, e.g., 15 µm–70 µm), nor patchy zoned crystals have been used. All the resulting timescales are reported in Table 3.

Method I indicates residence times of < 8.4 years. Method II is applicable to determine timescales of residence in ME1. The timescales obtained using Method II are on the order of years, with a maximum of 13.6 years in a crystal from felsic enclaves. A partial estimate of the uncertainties of an individual time determination is given by propagating the uncertainties in the determination of chemical composition (EMPA) and temperature (thermometry). As examples for the longest and the shortest determined timescales, the estimates yield, for the clinopyroxene 3 from the felsic enclaves, 13.6 (9.1–19.9) years and, for the clinopyroxene 9 from the hybrid enclave, 1.4 (0.8–2) years, where the times are given as in Table 3 and maximum and minimum errors based on the standard error of estimates of the thermometer (18.2 °C; Masotta et al. 2013) are given in brackets. On the same two crystals, in a similar scheme, the errors resulting from uncertainties on the chemical analysis (precision and accurancy = 1–5%) are 13.6 (10.7–15.8) years and 1.4 (0.8–1.8) years. However, as shown in Faak et al. (2014, 2015), the overall uncertainties are larger because of other unquantified sources of error (e.g. sectioning effects) and the best measure of uncertainty is the scatter of data from multiple determinations. Thus, from the data in Table 3, we infer that residence times of clinopyroxene crystals in the relevant magmatic environments (mainly ME1; Table 3) were on the order of years up to a decade or two. We do not make any attempts to distinguish between timescales obtained from different zoning- or rock- types. The implications of these timescales in the context of the plumbing system evolution are considered in the Discussion section.

Magma interaction dynamics

We simulated the mingling dynamics in a 2D rectangular box, considering two magma bodies separated by a horizontal unstable interface (Montagna et al. 2022). Results of numerical simulations described in Methods and in Online Resource 2 show efficient mingling dynamics between the two end-member magmatic components in the Zaro plumbing system. Due to the density contrast at the interface (Fig. 2), the buoyancy forces produce either a series of discrete plumes of shoshonitic magma in the trachytic one, in the low viscosity contrast scenario (Fig. 11a) or larger plumes, at high viscosity contrast (Fig. 11b). The initial gravitational instability causes the less dense shoshonitic end-member to rise towards the top of the system (Fig. 11).

On relatively short timescales of a few hours, the two magmas mingle very efficiently. Blobs of shoshonite rise into the residing trachyte, giving rise to typical mingling patterns very similar to those observed in the field (Fig. 1c). At both high and low viscosity contrasts, the results of modelling predict accumulation of mafic magma at the top of the plumbing system, as well as prolonged interactions among smaller and smaller shoshonitic blobs and the host trachyte. All simulation setup files and results are available in Montagna (2024).

Discussion

Magmatic processes in the Zaro plumbing system

The textural features, the isotopic differences and the chemical disequilibria detected by Pelullo et al. (2020) in the Zaro lavas and enclaves led the authors to hypothesize the injection of high temperature mafic magma into a trachytic magma reservoir. The trachytic magma (lava and felsic enclaves) had completely different Sr ($^{87}Sr/^{86}Sr = 0.70607–0.70615$) and Nd ($^{143}Nd/^{144}Nd = 0.51255–0.51256$) isotopic compositions compared to the mafic enclaves ($^{87}Sr/^{86}Sr = 0.70495–0.70500$; $^{143}Nd/^{144}Nd = 0.51268–0.51269$) and therefore the two cannot be directly genetically related (i.e. by simple fractional crystallization). Moreover, energy-constrained assimilation plus fractional crystallization modelling (Spera and Bohrson 2001) indicate that it is highly unlikely that the trachyte was derived from the shoshonitic melt (Pelullo et al. 2020). Hence, any evolution model of the Zaro plumbing system needs to consider the two distinct magmas as derived from different sources.

At the mineralogical scale, the detailed characterization of the Zaro clinopyroxene provides additional information on the processes that occurred in the plumbing system before eruption. Different compositions are well discernible in the clinopyroxene zoning pattern: ME2 (Mg# = 69–58)

Table 3 Timescale estimates for the Zaro clinopyroxene crystals derived from the different Fe–Mg diffusion modelling across selected profiles, calculated with different temperature values, depending on the output temperatures obtained for the compositional populations of the most external zone; c = core, m = mantle, r = rim

Lithotype	Cpx #	Zones	Mg# steps	Zoning type	T (°C)	Time (years)						Residence in
						Method I			Method II			
						first step (c-m)	last step (m-r)	total	first step (c-m)	last step (m-r)	total	
Lava	Cpx 5	c-r	75–69	Type IC	930			< 3.3				ME2
	Cpx 6	c-r	62–68	Type III	930			< 4.6				ME2
	Cpx 7	c-m-r	60–65–70	Type IA	962			< 4.3				ME1
		m-r	64–71	Type IA	962		< 0.9					ME1
	Cpx 8	c-m-r	75–64–75	Type ID	962					8.6		ME1
		c-m-r	75–64–75	Type ID	962					13.2		ME1
	Cpx 11	c-r	66–72	Type IA	962			< 2.9				ME1
		c-r	66–74	Type IA	962			< 2.5				ME1
Felsic	Cpx 1	c-r	69–76	Type IA	962						7.6	ME1
Enclaves	Cpx 2	c-m-r	75–72–76	Type III	962					9.2		ME1
	Cpx 3	c-r	69–75	Type IA	962						13.6	ME1
		c-r	69–75	Type IA	962						13.2	ME1
Hybrid	Cpx 1	c-m-r	75–84–76	Type II	1038			< 1.1				ME1
Enclave		m-r	84–76	Type II	1038		< 0.3					ME1
	Cpx 2	c-r	66–71	Type IA	1038						4.9	ME1
	Cpx 6	c-r	67–75	Type IA	1038						6.3	ME1
	Cpx 8	m-r	73–76	Type IA	1038		< 0.8					ME1
	Cpx 9	c-r	63–73	Type IA	1038						1.4	ME1
	Cpx 10	c-m-r	74–75–62	Type IC	930			< 8.4				ME2
Mafic	Cpx 3	m-r	83–77	Type II	1038					6.2		ME1
Enclaves		m-r	83–77	Type II	1038					3.3		ME1
	Cpx 8	c-r	66–76	Type IA	1038						3.7	ME1
		c-r	66–76	Type IA	1038						1.8	ME1
	Cpx 9	c-m-m-r	80–84-80–82–75	Type II	1038					4.3		ME1

Lithotype	n. of crystals	Upper limits of time	Residence time
Lava	5 (out of 13)	< 4.6 years	13.2–8.6 years
Felsic enclaves	3 (out of 3)		13.6–7.6 years
Hybrid enclave	6 (out of 10)	< 8.4 years	6.3–1.4 years
Mafic enclaves	3 (out of 9)		6.2–1.8 years

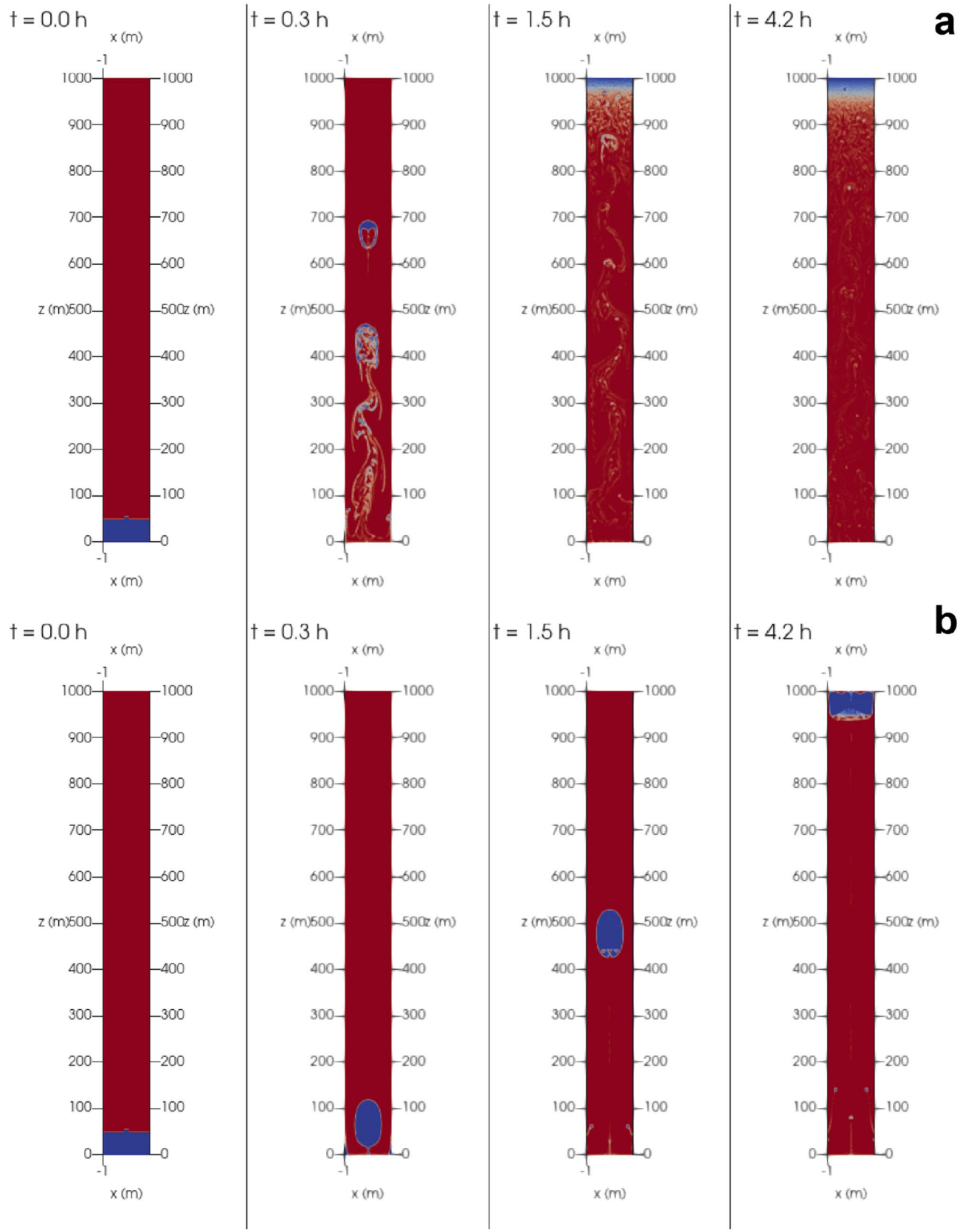

Fig. 11 Evolution of composition (in terms of end-members weight fractions) through time (t) in the simulated Zaro plumbing system: **a** setup with a low-viscosity, crystal-free trachytic end member; **b** setup with a high-viscosity, crystal-rich trachytic end-member

corresponds to the core composition of about half of the zoned crystals (Fig. 7), which are in equilibrium with the composition of evolved lavas (Fig. 10a), and hence likely represent phenocrysts grown in trachytic magma(s) stored at ~ 960–930 °C (Fig. 10b). The ME0 population (Mg# = 86–80), in equilibrium with shoshonitic melts (Fig. 10a), essentially present in the mantle of clinopyroxene of mafic enclaves, records crystallization in mafic magmas at high-T (~ 1120 °C; Fig. 10b). This is further supported by the notably high Cr content (Fig. 5c) of the Ischia mafic magmas.

The ME2 and ME0 populations represent a minor percentage in the Zaro clinopyroxene crystals, since all the unzoned crystals (58–73%), the frequent patchy zoned ones as well as each regularly zoned crystal (irrespective of the zoning type) have ME1 composition (Table 1; Figs. 6 and 7). This suggests that the ME1 was the dominant ME from which the clinopyroxene crystal cargo derives and points to the presence of a reservoir at depths corresponding to ~ 2–3 kbar and at temperatures of ~ 1040 °C (Table 2). The trachytic melt, from which clinopyroxenes with ME2 signature formed, can reside at a slightly shallower depth (~ 2 kbar) and/or may differ from ME1, being more evolved and cooler (~ 960–930 °C; Table 2). Considering the large uncertainties of the barometric estimates (Fig. 10b), the ME2 and ME1 environments can coexist at similar crustal levels as well. The most frequent compositional zoning in Type I clinopyroxenes (from ME2 to ME1 and vice-versa; Figs. 8 and 9) testifies the active communication between the two environments. It is important to note that no direct connectivity between ME0 and ME2 has been observed and that both converge to ME1 (Fig. 9). The compositionally intermediate ME1 signature in unzoned clinopyroxenes and at the *core* of differently zoned crystals (Fig. 6) can be reproduced by homogenization of mafic (ME0) and evolved (ME2) melts or can represent the composition of antecrysts. Also the chemical and isotopic disequilibria in clinopyroxenes from mafic enclaves (Fig. 10a; Pelullo et al. 2020) suggest that most of these crystals are antecrysts or formed as a consequence of mingling/mixing processes. In fact, in clinopyroxenes from mafic enclaves, the lack of ME0 rims (Fig. 6), the only composition in equilibrium with shoshonitic melts (Fig. 10a), as well as the lack of compositional zoning between ME0 and ME2 (Fig. 9), indicate that the ME0 population (detected almost exclusively in the mantles of Type II crystals) hardly crystallized from the same magma that subsequently formed the mafic enclaves. The chemical and isotopic mineral-melt equilibria testify that all olivines- and likely few pyroxenes- are phenocrysts of the mafic enclaves (Pelullo et al. 2020). Most likely, most of the clinopyroxene crystals, after their formation, were mechanically transported into the magma that originated the mafic enclaves. Hence, the clinopyroxene zoning pattern records processes older than the mingling possibly indicated by the occurrence of the mafic enclaves in the trachytic lavas.

Regardless of phenocrystic or antecrystic origin of the ME1 crystal cores, the ME0 population in Type II crystals (Fig. 9) testifies to the growth from a high-T mafic magma (Figs. 5c, 10b), consistent with mafic recharge into the ME1 environment. Consequences of this process are that (a) most pyroxenes with ME0 signatures grew as mantles on pre-existing ME1 cores and (b) some crystals were transferred from the mafic magma in the ME1 reservoir, explaining the rare occurrence of ME0 cores in Type II clinopyroxenes (Fig. 9). The occurrence of a large number of patchy zoned crystals (Table 1; Fig. 3b), as well as of resorbed cores (Online Resource 1), indicative of dissolution and recrystallization within the different MEs, is consistent with magma recharge, mixing and/or crystals cargo processes. The supply of mafic magma from depth interacting with a resident magma, or with pre-existing crystals, have been proved to produce resorption of crystals and zoning features (i.e. patchy zoning) indicating recycling dynamics (e.g., Streck 2008; Di Stefano et al. 2020; Petrone et al. 2022).

Hence, the ME1 reservoir is likely produced by mixing episodes due the new mafic melt supplied from depth and possibly dominates a section of the Zaro plumbing (Fig. 12a, b).

The frequent Type I and Type II crystals (Figs. 9, 12c) record movements between MEs at both boundaries (between the trachyte, possibly shallower, and the intermediate reservoir; and between the intermediate and the new input of mafic magma). It is important to note that the prevalence of the ME1 signature at the rims of most crystals (representing later crystallization stages; Figs. 6, 9), in different zoning types, suggests this was the last ME experienced by the crystals (for durations long enough to allow crystal growth) before eruption and quenching. Such signature in crystal rims is produced after i) a change in melt composition, i.e., for subsequent homogenization of ME0 and ME2 magmas, or ii) a change of one or some conditions, i.e., T, P, fO_2. Also, ME2 rims of the rare Type IC crystals indicate that some crystals resided and grew in the evolved trachytic environment before eruption. Moreover, reverse-to-normal or normal-to-reverse zoning in Type IB, Type ID, Type II and Type III (Figs. 8, 9), depict back and forth of crystals in different MEs, thus also suggesting a chaotic mixing regime, likely induced by the mafic recharge, a common feature in volcanic plumbing systems (e.g., Di Fiore et al. 2021; Petrone et al. 2022).

The interaction process of the input of mafic magma into the trachytic reservoir has been physically investigated through two-dimensional numerical simulations. This process produced convection and the rapid formation of discrete mafic blobs in the configurations predicted by the models (Fig. 11) and observed in the field (Fig. 1). We have

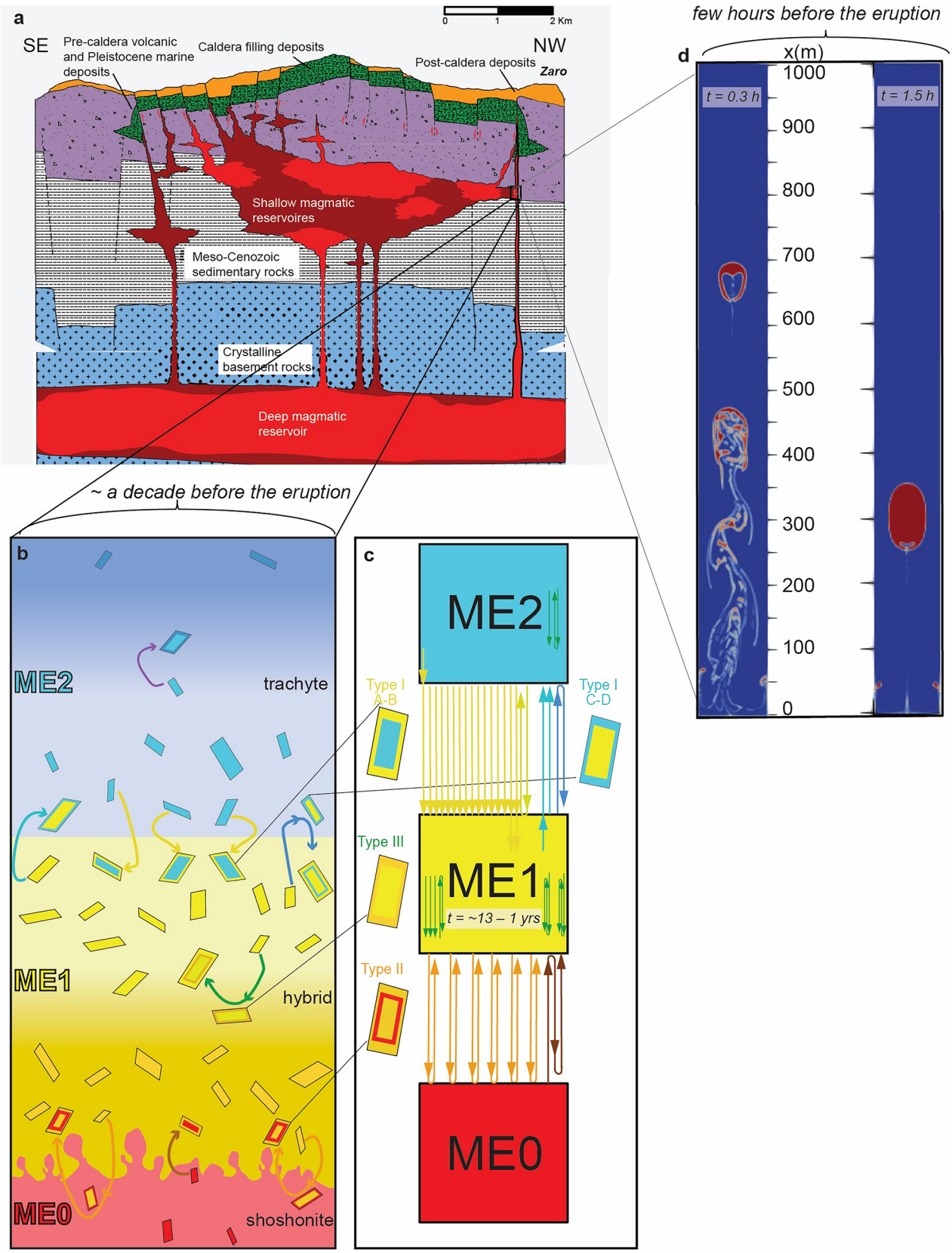
a
0
1
2 Km
SE
Pre-caldera volcanic and Pleistocene marine deposits
Caldera filling deposits
NW
Post-caldera deposits
Zaro
Shallow magmatic reservoires
Meso-Cenozoic sedimentary rocks
Crystalline basement rocks
Deep magmatic reservoir
~ a decade before the eruption
few hours before the eruption
b
ME2
trachyte
ME1
hybrid
ME0
shoshonite
c
ME2
Type I A-B
Type I C-D
Type III
ME1
t = ~13 – 1 yrs
Type II
ME0
d
x(m)
1000
900
800
700
600
500
400
300
200
100
0
t = 0.3 h
t = 1.5 h

◂**Fig. 12** Schematic sketch illustrating: **a** the Ischia deep system as inferred by geophysical and petrological data and geological models (depth not in scale; modified after Marotta et al. 2022); note that the sketch reproduces a structural setting and possible distribution of magmatic bodies between 2 and 6 km depth and reaching 8–10 km depth for the deep magmatic source, according to Marotta et al. (2022); the extension of the Ischia plumbing system is even much deeper according to D'Antonio et al. (2013) and Moretti et al. (2013); **b** the Zaro plumbing system in terms of the three distinct MEs detected in the clinopyroxene zoning pattern: the ME0, in red, in which clinopyroxenes with Mg# = 86–80 were formed, is associated with Ischia mafic (shoshonitic) magma(s); the ME2, in blue/light blue, in which clinopyroxenes with Mg# = 69–58 were formed, is associated with a trachytic reservoir; repeated input of ME0 and mixing with ME2 leads to the formation of the chemically intermediate (Mg# = 79–70), dominant ME1 long-lasting reservoir (in gold); the different colored curves indicate the passageways of crystals in the different MEs and correspond to those of Fig. 9; **c** the whole set of observed zoning patterns in the Zaro clinopyroxenes represented through the system analysis; the timescales obtained through diffusion modelling are reported; **d** frames of the numerical simulation of the input of mafic magma (mafic enclaves) in the trachytic reservoir (felsic lavas) occurred a few hours before the eruption

considered two setups, (i) a crystal-free setting (Fig. 11a) and (ii) one characterized by a much higher viscosity contrast, in which the trachytic melt contains 50 vol% of crystals (Fig. 11b), as observed in the lava. The evolution of the magma interaction in the Zaro plumbing system could have been somewhat intermediate between the two model setups, since there is evidence of (1) mixed/mingled magmas, due to more efficient interaction (Fig. 11a), preserved as hybrid enclaves and (2) magmas retained in their original shape, probably due to higher viscosity contrasts (Fig. 11b), preserved as mafic enclaves. The numerical simulations in this study calculate the evolution of a single pulse of magma input, but some features point to the fact that the overall evolution of the Zaro system may have involved many of such inputs. For example, the fact that some mafic input may have completely mixed to produce the hybrid enclaves, while others were preserved as mafic enclaves, points to input of magma at different times preserving different extents of mixing/mingling. Moreover, the sequential growth detected in Type II crystals can provide additional information on the sequence of the events: as stated before, the ME1 composition in crystal cores may result from mixing of mafic (ME0) and evolved (ME2) magmas. Similarly, subsequent mixing events could generate ME1 composition in most crystal rims, thus implying multiple pulses of mafic input at different evolutionary stages for core and rim formation. Finally, the last input is likely documented by the mafic enclaves themselves.

Temporal evolution of the plumbing system

When the information from crystal chemistry, compositional zoning and the available geochemical information (Pelullo et al. 2020) are considered together, they testify to a sequence of events that occurred in the plumbing system prior to the Zaro eruption. Moreover, the results of numerical simulations of physical mixing combined with those of diffusion modelling provide constraints on the duration of such events. The whole detected compositional variations and the calculated timescales are consistent with the occurrence of mafic (ME0) recharge processes in a trachytic (ME2) reservoir, that led to magma mingling presumably on timescales of hours (Fig. 11). Efficient magma mingling in reservoirs occurs much faster than chemical re-equilibration (Montagna et al. 2015) and thus the subsequent homogenization led to the formation of a dominant reservoir of intermediate composition (ME1). After mafic recharge, crystals have been stored for long times in the ME1 environment. For both Type I and Type II crystals, the durations and upper limit of times, obtained respectively at the core-rim and mantle-rim boundaries, are in the order of several years (mostly < 10 years, but up to 13 years; Table 3). These represent the time spent in the last magmatic environment prior to eruption. It is important to clarify the significance of these time estimates: these are *total* durations spent *in a given magmatic environment (most commonly ME1)*. If, for example, cold storage occurred in between two mafic inputs, that time interval would not show up in the estimates. Thus, the overall history may have been much longer than the decadal timescales that emerge from the records of zoning in clinopyroxenes, since these timescales are the total duration spent *at the conditions of ME1* (e.g. ~ 1040 °C). Such decadal timescales obtained by diffusion modelling are in agreement with other studies where enclaves were observed (e.g. Costa et al. 2003). Heterogeneities within the ME1 itself are sustained over this timescale as well. A situation where rapid mingling generates local environments within one of the major MEs would also explain how the interaction between these "sub-environments" could generate the compositional zoning in crystals where the entire compositional span lies within the compositional range of one ME (e.g. Type III; Fig. 8c). This last aspect is consistent with recent studies on magma mingling (Garg et al. 2019) that used numerical simulations similar to those performed in this work. These studies demonstrated that magma convection and mixing in a shallow magma chamber can result in long-lived, dynamically stable configurations with the coexistence of magmas from nearly pure to variably mixed end-member compositions, such as those detected in the Zaro rocks.

The hypothesized scenario implies that input of mafic melts from depth was common at Zaro for years to decades (or even longer if magma was stored at colder conditions in between) before eruption but did not cause its trigger; it is when such pulses exceeded some critical threshold (with or without additional influences, i.e. faults activation, volatile release) that eruption was triggered. Mafic enclaves offer the

record of quenched portions of mafic magmas included in a cooler more evolved melt (e.g., Martin et al. 2006; Zellmer and Turner 2007; Andrews and Manga 2014; Mariño et al. 2017). The Zaro mafic enclaves can represent a visual documentation of the final pulse because the numerical calculations of physical mixing indicate that they would form and accumulate at the top of the reservoir within a few hours, "freezing" the patterns observed in the field (Fig. 1c). This would also explain the lack of ME0 rims on the crystals, because a timescale of hours would have been too short for significant crystal growth. Such final pulse likely triggered the eruption on a few hours, as constrained by the numerical simulations of physical mixing (Fig. 11). However, the crystal cargo records older and longer processes. The ME1 composition, at rims of crystals, reflects the last prevailing environment in which the majority of crystals resided to allow crystal growth. The extended residence time within ME1, spanning several years (Table 3), underscores the complexity of magma dynamics.

This suggests that mixing between ME0 and ME2 may have repeatedly occurred without causing the eruption. Anyway, a final mixing event could have triggered the eruption, possibly when either a critical threshold was crossed, or additional external factors (e.g. fault activation, volatile release) occurred concurrently, carrying the overall clinopyroxene crystal cargo as well as remnants of incomplete mingling in the forms of trachytic, hybrid, and mafic enclaves.

Implications for hazard assessment

Mafic magma recharge and input in a shallow plumbing system involve migration of magma, volatiles and thermal energy that are able to cause effects driving unrest phases of active volcanoes (e.g., Aiuppa et al. 2022; Rosi et al. 2022). Nowadays, there is debate about involvement of mafic magma at shallow depth and related effects for the ongoing unrest phases at explosive volcanoes, such as the Campi Flegrei caldera (e.g., Chiodini et al. 2016; Buono et al. 2022). Although for Campi Flegrei and Ischia, linking petrological studies and monitoring signals (e.g., seismicity, ground deformation, gas emission; Saunders et al. 2012; Kahl et al 2011, 2013; Costa et al. 2013; Kilgour et al. 2014; Pankhurst et al. 2018; Nurfiani et al. 2021; Ostorero et al. 2022) is unattainable, due to the absence of past monitoring record, the investigation of magmatic processes and their timescales from products erupted in the recent past can yield information on the complex behavior of the plumbing system. This knowledge is useful to understand how the magmatic system is behaving at present or can behave in the future. Understanding this behavior, in conjunction with data from various monitoring systems, e.g. by geophysical methods, can be efficiently integrated with information from other case-studies at Ischia, or at similar active volcanoes worldwide to provide guidance for evaluating future volcanic hazards arising from magma transfer to shallower reservoirs.

Such insights are fundamental for accurately assessing volcanic hazards and formulating effective risk mitigation strategies. By elucidating the dynamics of these processes, we can enhance our ability to forecast volcanic activity and mitigate potential risks in densely inhabited active volcanic areas.

Conclusions

Chemically different magmas fed the north-western sector of Ischia island before the ~ 0.1 km^3 Zaro eruption that occurred 6.6 ± 2.2 ka ago. In a previous study, based on different chemical and isotopic features of the products, Pelullo et al. (2020) argued that two distinct magmatic components mingled in the Zaro magmatic system, one trachytic, the other shoshonitic. In this work, the different MEs detected in the clinopyroxene zoning pattern provide further evidence for the coexistence of compositionally distinct magmas, characterized by different sets of thermodynamic variables: ME2 (clinopyroxene Mg# = 69–58, trachytic melt at ~ 960–930 °C), ME0 (clinopyroxene Mg# = 86–80, mafic, shoshonitic melt at ~ 1120 °C) and a dominant intermediate composition, ME1 (clinopyroxene Mg# = 79–70, at ~ 1040 °C).

In addition to the previously detected chemical and isotopic variability, the investigation of zoning patterns of the Zaro clinopyroxene crystals sheds light on the sequence of processes involved in the plumbing system evolution, highlighting the occurrence of previous processes of mafic magma recharge and mixing.

Temporal information on the plumbing system evolution has been extracted by the combined use of numerical simulations and application of diffusion modelling to the clinopyroxene zoning pattern. The two methodologies provide insights on diverse aspects of the magmatic processes, operating at different temporal scales. The nature of compositional zoning indicates that the Zaro plumbing system developed by multiple episodes of mafic input over a timescale of about a decade or longer. Numerical modelling indicates that processes of magma mingling occur on rapid timescales of a few hours. Hence, it is likely that a final pulse of mafic magma, injected a few hours before the eruption, with or without the additional influence of external factors, such as faulting or volatile fluxing, may have tipped the system over some threshold, triggering the eruption.

Thus, the evolution of the plumbing system occurred over a range of timescales leading up to the eruption. Repeated short-lived events of magma mingling/mixing (probably lasting a few hours) led to the development of a dominant ME1 environment that persisted for decades or

longer before being likely interrupted by a final pulse of mafic magma injected and rapidly leading to the formation of enclaves before eruption. The intricate interplay among diverse pre-eruptive processes holds significant implications for understanding volcanic trigger mechanisms. Our work underscores the necessity of a detailed multi-methodological approach and of comprehensive analyses since a single event, such as an input of mafic magma, may variably influence the direct triggering of an eruption. Moreover, it emphasizes the importance of acquiring detailed information regarding the temporal dynamics of magma systems evolution. Associating this knowledge with the monitoring information is crucial for robust volcanic hazard assessment and implementing effective risk mitigation strategies.

Supplementary Information The online version contains supplementary material available at https://doi.org/10.1007/s00410-024-02138-9.

Acknowledgements This work has been partly developed during the "Timescales of magmatic processes and dynamic of plumbing system that feed volcanic eruptions revealed by minerals microanalysis: the case of the Neapolitan volcanoes", a project involving collaboration between INGV (Istituto Nazionale di Geofisica e Vulcanologia), the Department of Earth, Environment and Resources Sciences of the University of Naples Federico II and the Institute of Geology, Mineralogy und Geophysics of the Ruhr-Universität (Bochum, Germany). The INGV-OV laboratories have been financially supported by the EPOS Research Infrastructure through the contribution of the Italian Ministry of University and Research (MUR). Federico Brogi and Simone Colucci are gratefully thanked for their precious assistance in performing the numerical simulations models. Further support was provided by the project TIFEHO (Trachytic Ignimbrites magma-chambers Formation and Evolution in the pre-HOlocene history of the Campania volcanic area. Implications on magmatic processes, eruption dynamics, caldera collapse and resurgence), Resp. S. de Vita. Reviews by Chiara Maria Petrone and an anonymous reviewer, as well as comments and suggestions by Daniela Rubatto, Associated Editor of Contribution to Mineralogy and Petrology, greatly contributed to the improvement of the original manuscript and are kindly acknowledged.

Funding Open access funding provided by Istituto Nazionale di Geofisica e Vulcanologia within the CRUI-CARE Agreement. Funding was provided by German Academic Exchange Service (Grant Number: 57442045).

Data availability The data are available in the article and in the Online Supplementary Materials. Data on the simulation setup: https://doi.org/10.5281/zenodo.11085723.

Declarations

Conflict of interest The authors declare that they have no known competing financial interests or personal relationships that could have appeared to influence the work reported in this paper.

References

Aiuppa A, Bitetto M, Calabrese S, Delle Donne D, Lages J, La Monica FP, Chiodini G, Tamburello G, Cotterill A, Fulignati P, Gioncada A, Liu EJ, Moretti R, Pistolesi M (2022) Mafic magma feeds degassing unrest at Vulcano Island, Italy. Commun Earth Environ 3:255. https://doi.org/10.1038/s43247-022-00589-1

Allan ASR, Morgan DJ, Wilson CJN, Millet M-A (2013) From mush to eruption in centuries: assembly of the super-sized Oruanui magma body. Contrib Mineral Petrol 166:143–164. https://doi.org/10.1007/s00410-013-0869-2

Alves A, Janasi VD, Simonetti A, Heaman L (2009) Microgranitic enclaves as products of self-mixing events: a study of open-system processes in the Mauà granite, São Paulo, Brazil, based on in situ isotopic and trace elements in plagioclase. J Petrol 50:2221–2247. https://doi.org/10.1093/petrology/egp074

Andrews BJ, Manga M (2014) Thermal and rheological controls on the formation of mafic enclaves or banded pumice. Contrib Mineral Petrol 167:961. https://doi.org/10.1007/s00410-013-0961-7

Annen C (2009) From plutons to magma chambers: thermal constraints on the accumulation of eruptible silicic magma in the upper crust. Earth Planet Sci Lett 284:409–416. https://doi.org/10.1016/J.Epsl.2009.05.006

Aoki K-I, Shiba I (1973) Pyroxenes from lherzolite inclusions of Itinome-gata, Japan. Lithos 6:41–51. https://doi.org/10.1016/0024-4937(73)90078-9

Astbury RL, Petrelli M, Ubide T, Stock MJ, Arienzo I, D'Antonio M, Perugini D (2018) Tracking plumbing system dynamics at the Campi Flegrei caldera Italy: high-resolution trace element mapping of the Astroni crystal cargo. Lithos 318:464–477. https://doi.org/10.1016/j.lithos.2018.08.033

Bonechi B, Perinelli C, Gaeta M (2020) Clinopyroxene growth rates at high pressure: constraints on magma recharge of the deep reservoir of the Campi Flegrei Volcanic District (south Italy). Bull Volcanol 82:5. https://doi.org/10.1007/s00445-019-1342-5

Bonechi B, Perinelli C, Gaeta M, Stagno V, Fabbrizio A, Mollo S, Hrubiak R (2021) High pressure experimental investigation of clinopyroxene dissolution in a K-basaltic melt. Chem Geol 584:120533

Brogi F, Colucci S, Matrone J, Montagna CP, De' Michieli Vitturi M, Papale P, (2022) MagmaFOAM-1.0: a modular framework for the simulation of magmatic systems. Geosci Model Dev 15:3773–3796. https://doi.org/10.5194/gmd-15-3773-2022

Brown RJ, Orsi G, de Vita S (2008) New insights into Late Pleistocene explosive volcanic activity and caldera formation on Ischia (southern Italy). Bull Volcanol 70:583–603. https://doi.org/10.1007/s00445-007-0155-0

Brown RJ, Civetta L, Arienzo I, D'Antonio M, Moretti R, Orsi G, Tomlinson EL, Albert PG, Menzies MA (2014) Geochemical and isotopic insights into the assembly, evolution and disruption of a magmatic plumbing system before and after a cataclysmic caldera-collapse eruption at Ischia volcano (Italy). Contrib Mineral Petrol 168:1–23. https://doi.org/10.1007/s00410-014-1035-1

Buono G, Paonita A, Pappalardo L, Caliro S, Tramelli A, Chiodini G (2022) New insights into the recent magma dynamics under Campi Flegrei caldera (Italy) from petrological and geochemical

evidence. J Geophys Res Solid Earth 127:e2021JB023773. https://doi.org/10.1029/2021JB023773
Casalini M, Avanzinelli R, Heumann A, de Vita S, Sansivero F, Conticelli S, Tommasini S (2017) Geochemical and radiogenic isotope probes of Ischia volcano, southern Italy: constraints on magma chamber dynamics and residence time. Am Mineral 102:262–274. https://doi.org/10.2138/am-2017-5724
Chakraborty S, Ganguly J (1991) Compositional zoning and cation diffusion in garnets. In: Ganguly J (ed) Diffusion, atomic ordering, and mass transport: selected topics in geochemistry. Springer US, New York, pp 120–175
Chiodini G, Avino R, Brombach T, Caliro S, Cardellini C, de Vita S, Frondini F, Marotta E, Ventura G (2004) Fumarolic and diffuse soil degassing west of Mount Epomeo, Ischia (Italy). J Volcanol Geotherm Res 133:291–309. https://doi.org/10.1016/S0377-0273(03)00403-7
Chiodini G, Paonita A, Aiuppa A, Costa A, Caliro S, De Martino P, Acocella V, Vandemeulebrouck J (2016) Magmas near the critical degassing pressure drive volcanic unrest towards a critical state. Nat Commun 7:1–9. https://doi.org/10.1038/ncomms13712
Civetta L, Gallo G, Orsi G (1991) Sr- and Nd- isotope and trace-element constraints on the chemical evolution of the magmatic system of Ischia (Italy) in the last 55 ka. J Volcanol Geotherm Res 46:213–230. https://doi.org/10.1016/0377-0273(91)90084-D
Cooper KM (2019) Time scales and temperatures of crystal storage in magma reservoirs: implications for magma reservoir dynamics. Philos Trans R Soc 377:20180009. https://doi.org/10.1098/rsta.2018.0009
Costa F, Chakraborty S (2004) Decadal time gaps between mafic intrusion and silicic eruption obtained from chemical zoning patterns in olivine. Earth Planet Sci Lett 227:517–530. https://doi.org/10.1016/j.epsl.2004.08.011
Costa F, Chakraborty S, Dohmen R (2003) Diffusion coupling between trace and major elements and a model for calculation of magma residence times using plagioclase. Geochim Cosmochim Acta 67:2189–2200. https://doi.org/10.1016/S0016-7037(02)01345-5
Costa F, Dohmen R, Chakraborty S (2008) Time scales of magmatic processes from modeling zoning patterns of crystals. Rev Mineral Geochem 69:545–594. https://doi.org/10.2138/rmg.2008.69.14
Costa F, Andreastuti S, Bouvet de Maisonneuve C, Pallister JS (2013) Petrological insights into the storage conditions, and magmatic processes that yielded the centennial 2010 Merapi explosive eruption. J Volcanol Geotherm Res 261:209–235
Cubellis E, Ferri M, Luongo G (1995) Internal structures of Campi Flegrei caldera by gravimetric data. J Volcanol Geotherm Res 65:147–156. https://doi.org/10.1016/0377-0273(94)00047-K
D'Antonio M, Tonarini S, Arienzo I, Civetta L, Dallai L, Moretti R, Orsi G, Andria M, Trecalli A (2013) Mantle and crustal processes in the magmatism of the Campania region: inferences from mineralogy, geochemistry, and Sr–Nd–O isotopes of young hybrid volcanics of the Ischia island (South Italy). Contrib Mineral Petrol 165:1173–1194. https://doi.org/10.1007/s00410-013-0853-x
D'Antonio M, Arienzo I, Brown RJ, Petrosino P, Pelullo C, Giaccio B (2021) Petrography and mineral chemistry of Monte Epomeo Green Tuff, Ischia island, south Italy: Constraints for identification of the Y-7 tephrostratigraphic marker in distal sequences of the central Mediterranean. Minerals 11(9):955. https://doi.org/10.3390/min11090955
Davidson JP, Morgan DJ, Charlier BLA, Harlou R, Hora JM (2007) Microsampling and isotopic analysis of igneous rocks: Implications for the study of magmatic systems. Annu Rev Earth Planet Sci 35:273–311. https://doi.org/10.1146/annurev.earth.35.031306.140211
De Novellis V, Carlino S, Castaldo R, Tramelli A, De Luca C, Pino NA, Pepe S, Convertito V, Zinno I, De Martino P, Bonano M, Giudicepietro F, Casu F, Macedonio G, Manunta M, Cardaci C, Manzo M, Di Bucci D, Solaro G, Zeni G, Lanari R, Bianco F, Tizzani P (2018) The 21 August 2017 Ischia (Italy) earthquake source model inferred from seismological, GPS, and DInSAR measurements. Geophys Res Lett 45:2193–2202. https://doi.org/10.1002/2017GL076336
de Vita S, Sansivero F, Orsi G, Marotta E, Piochi M (2010) Volcanological and structural evolution of the Ischia resurgent caldera (Italy) over the past 10 ky. Geol Soc Am Spec Pap 464:193–239. https://doi.org/10.1130/2010.2464(10)
Di Fiore F, Mollo S, Vona A, MacDonald A, Ubide T, Nazzari M, Romano C, Scarlato P (2021) Kinetic partitioning of major and trace cations between clinopyroxene and phonotephritic melt under convective stirring conditions: New insights into clinopyroxene sector zoning and concentric zoning. Chem Geol 584:120531
Di Stefano F, Mollo S, Ubide T, Petrone CM, Caulfield J, Scarlato P, Nazzari M, Andronico D, Del Bello E (2020) Mush cannibalism and disruption recorded by clinopyroxene phenocrysts at Stromboli volcano: new insights from recent 2003–2017 activity. Lithos 360–361:105440
Dohmen R, Faak K, Blundy J (2017) Chronometry and speedometry of magmatic processes using chemical diffusion in olivine, plagioclase and pyroxenes. Rev Mineral Geochem 83:535–575
Druitt TH, Costa F, Deloule E, Dungan M, Scaillet B (2012) Decadal to monthly timescales of magma transfer and reservoir growth at a caldera volcano. Nature 482:77–80. https://doi.org/10.1038/nature10706
Dunworth E, Neumann ER, Rosenbaum J (2001) The Skien lavas, Oslo Rift: petrological disequilibrium and geochemical evolution. Contrib Mineral Petrol 140:701–719
Faak K, Coogan LA, Chakraborty S (2014) A new Mg-in-plagioclase geospeedometer for the determination of cooling rates of mafic rocks. Geochim Cosmochim Acta 140:691–707
Faak K, Coogan LA, Chakraborty S (2015) Near conductive cooling rates in the upper-plutonic section of crust formed at the East Pacific Rise. Earth Planet Sci Lett 423:36–47. https://doi.org/10.1016/j.epsl.2015.04.025
Fabbrocino S, Bellucci Sessa E, de Vita S, Di Vito MA, Avino R, Marotta E (2022) A GIS-based hydrogeological approach to the assessment of the groundwater circulation in the Ischia volcanic island (Italy). Front Earth Sci. https://doi.org/10.3389/feart.2022.883719
Flaherty T, Druitt TH, Tuffen H, Higgins MD, Costa F, Cadoux, (2018) Multiple timescale constraints for high-flux magma chamber assembly prior to the Late Bronze Age eruption of Santorini (Greece). Contrib Mineral Petrol 173:75. https://doi.org/10.1007/s00410-018-1490-1
Garg D, Papale P (2022) High-performance computing of 3D magma dynamics, and comparison with 2D simulation results. Front Earth Sci. https://doi.org/10.3389/feart.2021.760773
Garg D, Papale P, Colucci S, Longo A (2019) Long-lived compositional heterogeneities in magma chambers, and implications for volcanic hazard. Sci Rep 9:3321. https://doi.org/10.1038/s41598-019-40160-1
Ginibre C, Wörner G, Kronz A (2007) Crystal zoning as an archive for magma evolution. Elements 3:261–266. https://doi.org/10.2113/gselements.3.4.261
Gioncada A, Mazzuoli R, Milton AJ (2005) Magma mixing at Lipari (Aeolian Islands, Italy): insights from textural and compositional features of phenocrysts. J Volcanol Geotherm Res 145:97–118
Giudicepietro F, Ricciolino P, Bianco F, Caliro S, Cubellis E, D'Auria L, De Cesare W, De Martino P, Esposito AM, Galluzzo D,

Macedonio G, Lo Bascio D, Orazi M, Pappalardo L, Peluso R, Scarpato G, Tramelli A, Chiodini G (2021) Campi Flegrei, Vesuvius and Ischia seismicity in the context of the Neapolitan Volcanic Area. Front Earth Sci. https://doi.org/10.3389/feart.2021.662113

Grove TL, Bryan WB (1983) Fractionation of pyroxene-phyric MORB at low pressure: an experimental study. Contrib Mineral Petrol 84:293–209. https://doi.org/10.1007/BF01160283

Hildreth W, Wilson CJN (2007) Compositional zoning of the Bishop Tuff. J Petrol 48:951–999

Hughes GE, Petrone CM, Downes H, Varley NR, Hammond SJ (2021) Mush remobilisation and mafic recharge: a study of the crystal cargo of the 2013–17 eruption at Volcán de Colima, Mexico. J Volcanol Geothermal Res 416:107296. https://doi.org/10.1016/j.jvolgeores.2021.107296

Humphreys MCS, Blundy JD, Sparks RSJ (2006) Magma evolution and open-system processes at Shiveluch volcano: insights from phenocryst zoning. J Petrol 47:2303–2334. https://doi.org/10.1093/petrology/egl045

Iovine RS, Mazzeo FC, Arienzo I, D'Antonio M, Wörner G, Civetta L, Pastore Z, Orsi G (2017) Source and magmatic evolution inferred from geochemical and Sr-O-isotope data on hybrid lavas of Arso, the last eruption at Ischia island (Italy; 1302 AD). J Volcanol Geotherm Res 331:1–15. https://doi.org/10.1016/j.jvolgeores.2016.08.008

Jarosewich E, Nelen JA, Norberg JA (1980) Reference samples for electron microprobe analysis. Geostand Newsl 4:43–47. https://doi.org/10.1111/j.1751-908X.1980.tb00273.x

Kahl M, Chakraborty S, Costa F, Pompilio M (2011) Dynamic plumbing system beneath volcanoes revealed by kinetic modelling and the connection to monitoring data: an example from Mt Etna. Earth Planet Sci Lett 308:11–22. https://doi.org/10.1016/j.epsl.2011.05.008

Kahl M, Chakraborty S, Costa F, Pompilio M, Liuzzo M, Viccaro M (2013) Compositionally zoned crystals and realtime degassing data reveal changes in magma transfer dynamics during the 2006 summit eruptive episodes of Mt. Etna. Bull Volcanol 75:1–14. https://doi.org/10.1007/s00445-013-0692-7

Kahl M, Chakraborty S, Pompilio M, Costa F (2015) Constraints on the nature and evolution of the magma plumbing system of Mt Etna volcano (1991–2008) from a combined thermodynamic and kinetic modelling of the compositional record of minerals. J Petrol 56:2025–2068. https://doi.org/10.1093/petrology/egv063

Kent AJR, Darr C, Koleszar AM, Salisbury MJ, Cooper KM (2010) Preferential eruption of andesitic magmas through recharge filtering. Nat Geosci 3:631–636. https://doi.org/10.1038/ngeo924

Kilgour GN, Saunders KE, Blundy JD, Cashman KV, Scott BJ, Miller CA (2014) Timescales of magmatic processes at Ruapehu volcano from diffusion chronometry and their comparison to monitoring data. J Volcanol Geotherm Res 288:62–75. https://doi.org/10.1016/j.jvolgeores.2014.09.010

Mangler MF, Petrone CM, Hill S, Delgado-Granados H, Prytulak J (2020) A Pyroxenic view on magma hybridization and crystallization at Popocatépetl volcano, Mexico. Front Earth Sci. https://doi.org/10.3389/feart.2020.00362

Mangler MF, Petrone CM, Prytulak J (2022) Magma recharge patterns control eruption styles and magnitudes at Popocatépetl volcano (Mexico). Geology 50(3):366–370. https://doi.org/10.1130/G49365.1

Mariño PJ, Dobson KJ, Ortenzi G, Kueppers U, Morgavi D, Petrelli M, Hess K, Laeger K, Porreca M, Pimentel A, Perugini D (2017) Enhancement of eruption explosivity by heterogeneous bubble nucleation triggered by magma mingling. Sci Rep 7:16897. https://doi.org/10.1038/s41598-017-17098-3

Marotta E, de Vita S (2014) The role of pre-existing tectonic structures and magma chamber shape on the geometry of resurgent blocks: analogue models. J Volcanol Geotherm Res 272:23–38. https://doi.org/10.1016/j.jvolgeores.2013.12.005

Marotta E, Berrino G, de Vita S, Di Vito MA, Camacho AG (2022) Structural setting of the Ischia resurgent caldera (Southern Tyrrhenian Sea, Italy) by integrated 3D gravity inversion and geological models. In: Marotta E, D'Auria L, Zaniboni F, Nave R (eds) Volcanic Island: from hazard assessment to risk mitigation. Geological Society, London, Special Publications, p 519. https://doi.org/10.1144/SP519-2022-129

Martin VM, Holness MB, Pyle DM (2006) Textural analysis of magmatic enclaves from the Kameni Islands, Santorini, Greece. J Volcanol Geotherm Res 154:89–102. https://doi.org/10.1016/j.jvolgeores.2005.09.021

Masotta M, Mollo S, Freda C, Gaeta M, Moore G (2013) Clinopyroxene–liquid thermometers and barometers specificto alkaline differentiated magmas. Contrib Mineral Petrol 166:1545–1561. https://doi.org/10.1007/s00410-013-0927-9

Melluso L, Morra V, Guarino V, de'Gennaro R, Franciosi L, Grifa C (2014) The crystallization of shoshonitic to peralkaline trachyphonolitic magmas in a H_2O–Cl–F-rich environment at Ischia (Italy), with implications for the feeder system of the Campania Plain volcanoes. Lithos 210–211:242–259. https://doi.org/10.1016/j.lithos.2014.10.002

Mollo S, Putirka K, Misiti V, Soligo M, Scarlato P (2013) A new test for equilibrium based on clinopyroxene-melt pairs: clues on the solidification temperatures of Etnean alkaline melts on clinopyroxene- melt pairs: clues on the solidification temperatures of Etnean alkaline melts at post-eruptive conditions. Chem Geol 352:92–100. https://doi.org/10.1016/j.chemgeo.2013.05.026

Mollo S, Blundy J, Scarlato P, De Cristofaro SP, Tecchiato V, Di Stefano F, Vetere F, Holtz F, Bachmann O (2018) An integrated P-T-H2O-lattice strain model to quantify the role of clinopyroxene fractionation on REE+Y and HFSE patterns of mafic alkaline magmas: application to eruptions at Mt. Etna. Earth Sci Rev 185:32–56. https://doi.org/10.1016/j.earscirev.2018.05.014

Mollo S, Ubide T, Di Stefano F, Nazzari M, Scarlato P (2020) Polybaric/polythermalmagma transport and trace element partitioning recorded in single crystals: a case study of a zoned clinopyroxene from Mt. Etna. Lithos 356–357:105382

Montagna CP, Papale P, Longo A (2015) Timescales of mingling in shallow magmatic reservoirs. Chemical, physical and temporal evolution of magmatic systems. In: Caricchi L, Blundy JD (eds) Geological Society, London, Special Publications, pp 131–140. https://doi.org/10.1144/sp422.6

Montagna CP, Papale P, Longo A (2022) Magma chamber dynamics at the Campi Flegrei Caldera, Italy. In: Orsi G, D'Antonio M, Civetta L (eds) Campi Flegrei. Active volcanoes of the world. Springer, Berlin, pp 201–217. https://doi.org/10.1007/978-3-642-37060-1_7

Montagna C (2024) Pre-eruptive mingling simulation results - Zaro eruption, Ischia, *Zenodo*. https://doi.org/10.5281/zenodo.11085723

Moretti R, Arienzo I, Orsi G, Civetta L, D'Antonio M (2013) The deep plumbing system of Ischia: a physico-chemical window on the fluid-saturated and CO_2-sustained Neapolitan volcanism (southern Italy). J Petrol 54:951–984. https://doi.org/10.1093/petrology/egt002

Morgan DJ, Blake S (2006) Magmatic residence times of zoned phenocrysts: introduction and application of the binary element diffusion modeling (BEDM) technique. Contrib Mineral Petrol 151:58–70. https://doi.org/10.1007/s00410-005-0045-4

Morgan DJ, Blake S, Rogers NW, De Vivo B, Rolandi G, Macdonald R, Hawkesworth J (2004) Timescales of crystal residence and magma chamber volume from modeling of diffusion profiles in phenocrysts: Vesuvius 1944. Earth Planet Sci Lett 222:933–946

Morgan DJ, Blake S, Rogers NW, De Vivo B, Rolandi G, Davidson J (2006) Magma recharge at Vesuvius in the century prior to the eruption of A.D. 79. Geology 34:845–848

Müller T, Dohmen R, Becker HW, ter Heege J, Chakraborty S (2013) Fe–Mg interdiffusion rates in clinopyroxene: experimental data and implications for Fe–Mg exchange geothermometers. Contrib Mineral Petrol 166:1563–1576. https://doi.org/10.1007/s00410-013-0941-y

Nappi R, Alessio G, Gaudiosi G, Nave R, Marotta E, Siniscalchi V, Civico R, Pizzimenti L, Peluso R, Belviso P, Porfido S (2018) The 21 August 2017 md 4.0 Casamicciola earthquake: first evidence of coseismic normal surface faulting at the Ischia Volcanic Island. Seismol Res Lett 89:1323–1334. https://doi.org/10.1785/0220180063

Nappi R, Porfido S, Paganini E, Vezzoli L, Ferrario MF, Gaudiosi G, Alessio G, Michetti AM (2021) The 2017, MD = 4.0, Casamicciola earthquake: ESI-07 scale evaluation and implications for the source model. Geoscience 11:44. https://doi.org/10.3390/geosciences11020044

Neave DA, Maclennan J (2020) Clinopyroxene dissolution records rapid magma ascent. Front Earth Sci 8:188. https://doi.org/10.3389/feart.2020.00188

Nurfiani D, Wang X, Gunawan H, Triastuty H, Hidayat D, Wei SJ, Taisne B, Bouvet de Maisonneuve C (2021) Combining petrology and seismology to unravel the plumbing system of a typical arc volcano: an example from Marapi, West Sumatra, Indonesia. Geochem Geophys Geosys 2:2. https://doi.org/10.1029/2020GC009524

Orsi G, Piochi M, Campajola L, D'Onofrio A, Gialanella L, Terrasi F (1996) ^{14}C geochronological constraints for the volcanic history of the island of Ischia (Italy) over the last 5000 years. J Volcanol Geotherm Res 71:249–257. https://doi.org/10.1016/0377-0273(95)00067-4

Orsi G, de Vita S, Di Vito M, Isaia R, Nave R, Heiken G (2003) Facing volcanic and related hazards in the Neapolitan Area. In: Heiken G, Fakundiny R, Sutter J (eds) Earth science in the cities: a reader. American Geophysical Union book, Washington, pp 121–170. https://doi.org/10.1029/SP056p0187

Ostorero L, Balcone-Boissard H, Boudon G, Nikolai M, Shapiro NM, Belousov A, Belousova M, Auer A, Senyukov SL, Droznina SY (2022) Correlated petrology and seismicity indicate rapid magma accumulation prior to eruption of Kizimen volcano, Kamchatka. Commun Earth Environ 3:290. https://doi.org/10.1038/s43247-022-00622-3

Palummo F, Mollo S, Petrone CM, Ellis BS, De Astis G, Nazzari M, Scarlato P, Bachmann O (2021) Decoding multiple zoning patterns in clinopyroxene phenocrysts at Vulcano Island: a record of dynamic crystallization through interconnected reservoirs. Lithos 406:106517

Pankhurst MJ, Morgan DJ, Thordarson T, Loughlin SC (2018) Magmatic crystal records in time, space, and process, causatively linked with volcanic unrest. Earth Planet Sci Lett 493:231–241

Pelullo C, Cirillo G, Iovine RS, Arienzo I, Aulinas P, Petrosino P, Fernandez-Turiel JL, D'Antonio M (2020) Geochemical and Sr–Nd isotopic features of the Zaro volcanic complex: insights on the magmatic processes triggering a small-scale prehistoric eruption at Ischia island (south Italy). Int J Earth Sci 109:2829–2849. https://doi.org/10.1007/s00531-020-01933-6

Pelullo C, Chakraborty S, Cambeses A, Dohmen R, Arienzo I, D'Antonio M, Pappalardo L, Petrosino P (2022) Insights into the temporal evolution of magma plumbing systems from compositional zoning in clinopyroxene crystals from the Agnano-Monte Spina Plinian eruption (Campi Flegrei, Italy). Geochim Cosmochim Acta 328:185–206. https://doi.org/10.1016/j.gca.2022.04.007

Petrelli M, Ágreda López M, Pisello A, Perugini D (2023) Pre-eruptive dynamics at the Campi Flegrei Caldera: from evidence of magma mixing to timescales estimates. Earth Planets Space 75:19. https://doi.org/10.1186/s40623-023-01765-z

Petrone C, Bugatti G, Braschi E, Tommasini S (2016) Pre-eruptive magmatic processes re-timed using a non-isothermal approach to magma chamber dynamics. Nat Commun 7:12946. https://doi.org/10.1038/ncomms12946

Petrone CM, Braschi E, Francalanci L, Casalini M, Tommasini S (2018) Rapid mixing and short storage timescale in the magma dynamics of a steady-state volcano. Earth Planet Sci Lett 492:206–221

Petrone CM, Mollo S, Gertisser R, Buret Y, Scarlato P, Del Bello E, Andronico D, Ellis B, Pontesilli A, De Astis G, Giacomoni PP, Coltorti M, Reagan M (2022) Magma recharge and mush rejuvenation drive paroxysmal activity at Stromboli volcano. Nat Commun 13:7717. https://doi.org/10.1038/s41467-022-35405-z

Piochi M, Civetta L, Orsi G (1999) Mingling in the magmatic system of Ischia (Italy) in the past 5 ka. Mineral Petrol 66:227–258. https://doi.org/10.1007/BF01164495

Poli S, Chiesa S, Gillot PY, Gregnanin A, Guichard F (1987) Chemistry versus time in the volcanic complex of Ischia (Gulf of Naples, Italy): evidence of successive magmatic cycles. Contrib Mineral Petrol 95:322–335. https://doi.org/10.1007/BF00371846

Putirka KD (2008) Thermometers and barometers for volcanic systems. Rev Mineral Geochem 69:61–120. https://doi.org/10.2138/rmg.2008.69.3

Putirka KD, Johnson M, Kinzler RJ, Longhi J, Walker D (1996) Thermobarometry of mafic igneous rocks based on clinopyroxene-liquid equilibria, 0–30 kbar. Contrib Mineral Petrol 123:9–108

Putirka KD, Mikaelian H, Ryerson F, Shaw H (2003) New clinopyroxene–liquid thermobarometers for mafic, evolved, and volatile-bearing lava compositions, with applications to lavas from Tibet and the Snake River Plain, Idaho. Am Mineral 88:1542–1554. https://doi.org/10.2138/am-2003-1017

Rosi M, Acocella V, Cioni R, Bianco F, Costa A, De Martino P, Giordano G, Inguaggiato S (2022) Defining the pre-eruptive states of active volcanoes for improving eruption forecasting. Front Earth Sci 10:795700. https://doi.org/10.3389/feart.2022.795700

Saunders K, Blundy J, Dohmen CK (2012) Linking petrology and seismology at an active volcano. Science 336:1023–1027

Sbrana A, Marianelli P, Pasquini G (2018) Volcanology of Ischia (Italy). J Maps 14:494–503. https://doi.org/10.1080/17445647.2018.1498811

Selva J, Acocella V, Bisson M, Caliro S, Costa A, Della Seta M, De Martino P, de Vita S, Federico C, Giordano G, Martino S, Cardaci C (2019) Multiple natural hazards at volcanic islands: a review for the Ischia volcano (Italy). J Appl Volcan 8:1–43. https://doi.org/10.1186/s13617-019-0086-4

Seyler M, Bonatti E (1994) Na, Al^{IV} and Al^{VI} in clinopyroxenes of subcontinental and suboceanic ridge peridotites: a clue to different melting processes in the mantle? Earth Planet Sci Lett 122:281–289. https://doi.org/10.1016/0012-821X(94)90002-7

Solaro C, Balcone-Boissard H, Morgan DJ, Boudon G, Martel C, Ostorero L (2020) A system dynamics approach to understanding the deep magma plumbing system beneath Dominica (Lesser Antilles). Front Earth Sci. https://doi.org/10.3389/feart.2020.574032

Sparks RSJ, Cashman KV (2017) Dynamic magma systems: implications for forecasting volcanic activity. Elements 13:35–40. https://doi.org/10.2113/gselements.13.1.35

Spera FJ, Bohrson WA (2001) Energy-constrained open-system magmatic processes I: general model and energy-constrained

assimilation and fractional crystallization (EC-AFC) formulation. J Petrol 42:999–1018. https://doi.org/10.1093/petrology/42.5.999

Streck MJ (2008) Mineral textures and zoning as evidence for open system processes. Rev Mineral Geochem 69:595–622. https://doi.org/10.2138/rmg.2008.69.15

Trasatti E, Acocella V, Di Vito MA, Del Gaudio C, Weber G, Aquino I, Caliro S, Chiodini G, de Vita S, Ricco C, Caricchi L (2019) Magma degassing as a source of long-term seismicity at volcanoes: the Ischia Island (Italy) case. Geophys Res Lett 46:14421–14429. https://doi.org/10.1029/2019GL085371

Trepmann CA, Stöckhert B, Chakraborty S (2004) Oligocene trondhjemitic dikes in the Austroalpine basement of the Pfunderer Berge Südtirol—level of emplacement and metamorphic overprint. Eur J Mineral 16:641–659. https://doi.org/10.1127/0935-1221/2004/0016-0641

Ubide T, Kamber BS (2018) Volcanic crystals as time capsules of eruption history. Nat Commun 9:326. https://doi.org/10.1038/s41467-017-02274-w

Ubide T, McKenna CA, Chew DM, Kamber BS (2015) High-resolution LA-ICP-MS trace element mapping of igneous minerals: in search of magma histories. Chem Geol 409:157–168. https://doi.org/10.1016/j.chemgeo.2015.05.020

Ubide T, Mollo S, Zhao JX, Nazzari M, Scarlato P (2019) Sector zoned clinopyroxene as a recorder of magma history, eruption triggers, and ascent rates. Geochim Cosmochim Acta 251:265–283. https://doi.org/10.1016/j.gca.2019.02.021

Vezzoli L (1988) Island of Ischia. Quaderni de La Ricerca Scientifica. Consiglio Nazionale delle Ricerche, Rome

Vezzoli L, Principe C, Malfatti J, Arrighi S, Tanguy J, Le Goff M (2009) Modes and times of caldera resurgence: The <10 ka evolution of Ischia Caldera, Italy, from high-precision archaeomagnetic dating. J Volcanol Geotherm Res 186:305–319. https://doi.org/10.1016/j.jvolgeores.2009.07.008

Wallace GS, Bergantz GW (2002) Wavelet-based correlation (WBC) of zoned crystal populations and magma mixing. Earth Planet Sci Lett 202:133–145. https://doi.org/10.1016/S0012-821X(02)00762-8

Wallace GS, Bergantz GW (2004) Constraints on mingling of crystal populations from off-center zoning profiles: a statistical approach. Am Mineral 89:64–73. https://doi.org/10.2138/am-2004-0109

Wang X, Hou T, Wang M, Zhang C, Zhang Z, Pan R, Marxer F, Zhang H (2021) A new clinopyroxene thermobarometer for mafic to intermediate magmatic systems. Eur J Mineral 33:621–637. https://doi.org/10.5194/ejm-33-621-2021

Wass SY (1979) Multiple origins of clinopyroxenes in alkali basaltic rocks. Lithos 12:115–132. https://doi.org/10.1016/0024-4937(79)90043-4

Zellmer GF, Turner SP (2007) Arc dacite genesis pathways: evidence from mafic enclaves and their hosts in Aegean lavas. Lithos 95:346–362. https://doi.org/10.1016/j.lithos.2006.08.002

Zellmer GF, Blake S, Vance D, Hawkesworth C, Turner S (1999) Plagioclase residence times at two island arc volcanoes (Kameni Islands, Santorini, and Soufriere, St. Vincent) determined by Sr diffusion systematics. Contrib Mineral Petrol 136:345–357. https://doi.org/10.1007/s004100050543

Zellmer GF, Sparks RSJ, Hawkesworth CJ, Wiedenbeck M (2003) Magma emplacement and remobilization timescales beneath Montserrat: insights from Sr and Ba zonation in plagioclase phenocrysts. J Petrol 44:1413–1431. https://doi.org/10.1093/petrology/44.8.1413